

1 **Model-driven experimental design identifies counter-acting feedback
2 regulation in the osmotic stress response of yeast**

3 Sara Kimiko Suzuki¹, Beverly Errede², Henrik G. Dohlman^{1,3,*}, Timothy C. Elston^{1,3,4,†}

4 ¹Curriculum in Bioinformatics and Computational Biology, UNC School of Medicine, Chapel Hill,
5 North Carolina, USA.

6 ²Department of Biochemistry and Biophysics, UNC School of Medicine, Chapel Hill, North
7 Carolina, USA.

8 ³Department of Pharmacology, UNC School of Medicine, Chapel Hill, North Carolina, USA.

9 ⁴Computational Medicine Program, UNC School of Medicine, Chapel Hill, North Carolina, USA.

10 *Correspondence: hdohlman@med.unc.edu

11 †Correspondence: Timothy_elston@med.unc.edu

12 **Keywords:** modeling, systems biology, phosphorylation, MAPK, HOG pathway, yeast, feedback

13

14

15

16

17

18

19

20

21

22

23

24

25 **Conflict of interest statement:** The authors declare no potential conflict of interest.

26 **Abstract**

27 Cells rely on mitogen-activated protein kinases (MAPKs) to survive environmental stress. In
28 yeast, activation of the MAPK Hog1 is known to mediate the response to high osmotic
29 conditions. Recent studies of Hog1 revealed that its temporal activity is subject to both negative
30 and positive feedback regulation, yet the mechanisms of feedback remain unclear. By designing
31 mathematical models of increasing complexity for the Hog1 MAPK cascade, we identified
32 pathway circuitry sufficient to capture Hog1 dynamics observed *in vivo*. We used these models
33 to optimize experimental designs for distinguishing potential feedback loops. Performing
34 experiments based on these models revealed mutual inhibition between Hog1 and its
35 phosphatases as the likely positive feedback mechanism underlying switch-like, dose-
36 dependent MAPK activation. Importantly, our findings reveal a new signaling function for MAPK
37 phosphatases. More broadly, they demonstrate the value using mathematical models to infer
38 targets of feedback regulation in signaling pathways.

39

40

41

42

43

44

45

46

47

48

49

50

51 **Introduction**

52 All cells rely on intracellular signaling systems to protect themselves from environmental
53 stress. These pathways execute the appropriate cellular response by relaying the strength,
54 duration, and other quantitative information about changing environmental conditions (Alon,
55 2007; Purvis and Lahav, 2013). When the external stimulus is harmful to the cell, the cell's
56 response can determine whether it survives. To mitigate the effects of stress, cells use signaling
57 pathways that often incorporate mitogen-activated protein kinase (MAPK) cascades (Carnello
58 and Roux, 2011). In this three-tiered signaling motif, a MAPK kinase kinase (MAP3K)
59 phosphorylates a MAPK kinase (MAP2K), which in turn phosphorylates a terminal MAPK.
60 These phosphorylation events occur within the activation loop of the kinase domain, thereby
61 enabling catalytic activity. The MAPK coordinates all events required for a proper response to
62 the environmental stress.

63 The MAPK signaling cascade is conserved in all eukaryotic organisms, from humans to
64 yeast. In the case of the *S. cerevisiae* High Osmolarity Glycerol (HOG) pathway, hyperosmotic
65 stress initiates signaling to activate cytoprotective responses (Brewster and Gustin, 2014;
66 Miermont et al., 2011; O'Rourke et al., 2002; Saito and Posas, 2012). This signaling occurs
67 through the Sln1 and Sho1 input branches where the Sln1 branch has two MAP3Ks, Ssk2 and
68 Ssk22, while the Sho1 branch has a single MAP3K, Ste11 (Figure 1). All three of these MAP3Ks
69 converge on and activate the MAP2K Pbs2, while Pbs2 alone activates the MAPK Hog1. Hog1
70 protects the cell by increasing cytosolic osmolyte concentrations to reestablish turgor pressure
71 over time. Hog1 is known to phosphorylate at least 35 proteins, some of which are transcription
72 factors in the nucleus leading to the induction or repression of ~300 genes (Capaldi et al., 2008;
73 Janschitz et al., 2019; O'Rourke and Herskowitz, 2004). Activation of this pathway is transient,
74 and once cells have fully-adapted, they can resume cell cycle progression and proliferation
75 (Escoté et al., 2011).

76 Many MAPK signaling networks rely on feedback regulation to amplify or diminish a
77 signal in a time-dependent manner (Albeck et al., 2013; Brandman and Meyer, 2008). While
78 multiple feedback loops have been identified for the HOG pathway, it is unknown how these
79 regulatory mechanisms function together or if they are sufficient to capture the dynamics of
80 Hog1 activity. For example, Hog1 phosphorylates the osmosensor Sho1 and the MAP3K Ssk2,
81 leading to diminished signal transduction (Hao et al., 2007; Sharifian et al., 2015). Similarly,
82 Hog1-dependent phosphorylation of Ste50, the adapter protein of Ste11, increases Ste50
83 dissociation from its signaling complex, thereby downregulating signal transmission (Nagiec and
84 Dohlman, 2012; Yamamoto et al., 2010). Hog1-dependent activity also attenuates signaling by
85 initiating the closure of osmolyte channels, inducing the synthesis of amino acid metabolites,
86 increasing the production of osmolytes like glycerol and trehalose, and inducing the transcription
87 of osmolyte metabolism-associated genes (Babazadeh et al., 2014; Lee et al., 2013; O'Rourke
88 and Herskowitz, 2004; Petelenz-Kurdziel et al., 2013; Shellhammer et al., 2017).
89 Phosphorylation and osmolyte accumulation act on different timescales to suppress Hog1
90 signaling, and therefore could differentially affect the dynamics of Hog1 activity.

91 Further studies have shown that Hog1 acts, in part, by regulating its own catalytic
92 activity. In response to a wide range of external salt concentrations, Hog1 is rapidly and fully
93 phosphorylated, whereas dephosphorylation occurs at increasingly later times as the dose of
94 the stimulus increases (English et al., 2015). Because different doses of salt elicit different
95 transcriptional responses, it is likely that signal duration, rather than amplitude, transmits
96 information regarding the external salt concentration. This behavior has been referred to as
97 “dose-to-duration” signaling (Behar et al., 2008). Experiments using a Hog1 variant (Hog1-as)
98 engineered to respond to a pharmacological inhibitor (Klein et al., 2011; Westfall and Thorner,
99 2006) revealed that Hog1 kinase activity affects its response to high osmotic stress. In the
100 absence of MAPK kinase activity, the maximal level of Hog1 phosphorylation is dependent on
101 the concentration of external osmolytes; peak phosphorylation is delayed and is far more

102 sustained than that of the wildtype MAPK (English et al., 2015). These observations indicate
103 that Hog1 kinase activity is required for full activation by the MAP2K Pbs2 and for timely
104 inactivation by appropriate phosphatases. Such behaviors are indicative of positive and
105 negative feedback. However, while the necessity of feedback within the HOG pathway has long
106 been appreciated, many details of the mechanisms controlling Hog1 phosphorylation dynamics
107 are still unknown. This is in part due to the complexities of the observed behaviors, which are
108 both dose- and time-dependent.

109 One approach to understanding complex biological data is to describe them using
110 mathematical models. The structures of HOG pathway models have varied substantially, from
111 having minimal two state systems to representing all of the HOG pathway components (Klipp
112 and Schaber, 2008; Mitchell et al., 2015; Stojanovski et al., 2017). A subset has focused on
113 negative feedback while others have investigated the role of the two input branches (Granados
114 et al., 2017; Hersen et al., 2008; Schaber et al., 2012). Many models investigating feedback
115 regulation concluded that the pathway needs Hog1-dependent integral negative feedback
116 control to exhibit perfect adaptation (Klipp et al., 2005; Mettetal et al., 2008; Mitchell et al., 2015;
117 Muzzey et al., 2009; Zi et al., 2010). Other models further explored different mechanisms of
118 negative feedback, proposing that the required feedback mechanism entails the slow
119 accumulation of osmolytes (Petelenz-Kurdziel et al., 2013; Schaber et al., 2012). Subsequently,
120 our experimental efforts revealed the potential importance of positive feedback for fast Hog1
121 activation (English et al., 2015). However, there are no reported mechanisms of positive
122 feedback for the HOG pathway.

123 Despite substantial progress, a complete systems-level understanding for the role of
124 counter-acting feedback regulation is still lacking. Therefore, our goal here was to perform a
125 systematic computational analysis of Hog1 activity that could identify likely targets of feedback
126 regulation and to then design experiments to test the predicted feedback loops. The starting
127 point for our investigations was a model of a three-tiered MAPK cascade to which we

128 systematically added different potential feedback motifs. In particular, we started with a minimal
129 model for adaptation involving a single negative feedback loop (Ferrell, 2016), and added
130 candidate feedback loops until we were able to reproduce Hog1 phosphorylation dynamics.
131 Combining both modeling and biological experiments allowed us to identify the necessary
132 feedback mechanisms by using each method to inform the other in an iterative process. As
133 detailed below, our investigations determined that fast positive feedback and delayed negative
134 feedback can account for the time- and dose-dependent behaviors of Hog1. Further analysis
135 suggests that positive feedback is controlled by Hog1 down regulation of its phosphatase
136 activity.

137

138 **Results**

139 **Hog1 and Pbs2 phosphorylation are dependent on Hog1 kinase activity**

140 Our broad objective is to identify pathway circuitry for regulating MAPK signaling
141 generally, and for the HOG pathway in particular. We first collected the experimental data
142 depicting pathway dynamics. Our approach was to design time-course experiments that
143 measure the dynamics of Hog1 and its upstream kinase, Pbs2, under various experimental
144 conditions. Using this approach, we defined 10 important characteristics of the HOG pathway
145 that our models need to capture in order to be biologically accurate. These 10 characteristics
146 are enumerated in the following section and are summarized below.

147 We first assessed Hog1 phosphorylation upon hyperosmotic stress. We exposed liquid
148 cultures to a range of KCl concentrations and collected whole-cell lysates over time. To quantify
149 the proportion of phosphorylated Hog1, we used Phos-tag immunoblotting, which resolves
150 different states of a protein in proportion to the number of sites phosphorylated (Kinoshita et al.,
151 2006). Because wildtype Hog1 is normally either unphosphorylated or dually phosphorylated,
152 we can easily distinguish the two forms of the protein after SDS-PAGE with the Phos-tag

153 reagent (Figure 2A, left). The stoichiometry of phosphorylation was calculated as the proportion
154 of dually phosphorylated Hog1 compared to the total amount of Hog1 in each lane (Figure 2A,
155 right). Consistent with previous results (English et al., 2015), we observed three characteristic
156 features of Hog1: (1) no basal activation, (2) fast and full activation in response to KCl, and (3)
157 transient duration of activation that is proportional to the KCl dose. These features give rise to
158 dose-to-duration signaling.

159 Hog1 kinase activity can be selectively blocked using an analog-sensitive Hog1 variant
160 ($\text{Hog1}^{\text{T}100\text{A}}$) that is inhibited with the ATP analog, [1-(1,1-dimethylethyl)-3-(1-naphthalenyl)1H-
161 pyrazolo[3,4-d]pyrimidin-4-amine] or 1-NA-PP1 (Kung et al., 2006). Accordingly, we stimulated
162 cells following $\text{Hog1}^{\text{T}100\text{A}}$ inhibition, and ran Phos-tag SDS-PAGE as previously described
163 (English et al., 2015). Inhibited Hog1 (Hog1-as) exhibited three characteristics that differ from
164 wildtype. Consistent with results of English et al. (2015), we observed Hog1 dynamics that were:
165 (4) slow and (5) sustained (Figure 2B). The slowed rate of activation and lack of full dual
166 phosphorylation when Hog1 is inhibited indicates the presence of Hog1-dependent positive
167 feedback. Furthermore, as noted previously, Hog1 exhibits basal dual phosphorylation when its
168 kinase activity is inhibited (English et al., 2015; Macia et al., 2009; Schaber et al., 2012). Our
169 quantification revealed that under these conditions dually phosphorylated Hog1 slowly
170 accumulates, reaching a steady state of approximately 30% of the total (characteristic feature
171 (6)) (Figure 2C). The lack of signal attenuation and increase in the basal level of dually
172 phosphorylated Hog1 in the absence of Hog1 activity demonstrate Hog1-dependent negative
173 feedback. These results reflect the complexity of HOG signaling and motivate our investigations
174 to determine where in the pathway feedback regulation acts.

175 We next measured the dynamics of another upstream signaling component, at multiple
176 salt concentrations, with and without Hog1 kinase inhibition. Our rationale was that these
177 experiments would provide important additional data for informing our models and identifying
178 targets of feedback regulation. We chose the MAP2K Pbs2 because it is more abundant than

179 any one of the MAP3Ks, is common to both input branches of the pathway and is
180 phosphorylated when activated (Tatebayashi et al., 2020). Thus, we used the Phos-tag western
181 blotting technique described above to measure the dose- and Hog1-kinase dependency of Pbs2
182 phosphorylation dynamics. As shown in Figure 2D, osmotic stress stimulation caused a mobility
183 shift of Pbs2 that was (7) fast and partial and also (8) transient. This behavior mirrored two of
184 the wildtype properties, but unlike Hog1, Pbs2 did not become fully phosphorylated at 150 mM
185 KCl. When Hog1 was kinase-inhibited, Pbs2 phosphorylation was also (9) fast and partial, but
186 (10) sustained, as observed for Hog1-as, indicating signal attenuation occurs earlier in the
187 pathway.

188

189 **Delayed negative feedback promotes pathway deactivation**

190 Our next step was to identify potential HOG feedback circuits by fitting models to our
191 Hog1 and Pbs2 phosphorylation data. We considered a model successful if it could capture the
192 10 pathway characteristics enumerated above. We took a systematic approach by beginning
193 with a minimal model for adaptive behavior and adding complexity as needed. In this way, we
194 hoped to gain insight to the limitations of each model. The minimal model (Model I) for the HOG
195 MAPK cascade is comprised of a single negative feedback loop initiating from Hog1 and
196 targeting the MAP3K (Figure 3A). From a biological perspective, this model represents Hog1
197 suppressing its own activity by diminishing the rate at which the MAP3K is activated, this might
198 occur through increasing the intracellular osmolyte concentration, feedback phosphorylation or
199 both (English et al., 2015; Hao et al., 2007; Sharifian et al., 2015). The model consists of three
200 species, representing each of the three kinases in the MAPK cascade. We modeled
201 phosphorylation and dephosphorylation using Michaelis-Menten kinetics and ignored the
202 synthesis and degradation of the kinases, as their expression is not known to be induced
203 following hyperosmotic stress.

204 *Model I* (Figure 3A):

205
$$\frac{dMAP3K}{dt} = \frac{1}{\left(1 + \frac{Hog1}{\beta}\right)} \cdot \left(\frac{k_b + k_1 \cdot KCl}{K_1 + MAP3K_I}\right) MAP3K_I - \frac{k_2 \cdot MAP3K}{K_2 + MAP3K} \quad (1)$$

206
$$\frac{dPbs2}{dt} = \frac{k_3 \cdot MAP3K \cdot Pbs2_I}{K_3 + Pbs2_I} - \frac{k_4 \cdot Pbs2}{K_4 + Pbs2} \quad (2)$$

207
$$\frac{dHog1}{dt} = \frac{k_5 \cdot Pbs2 \cdot Hog1_I}{K_5 + Hog1_I} - \frac{k_6 \cdot Hog1}{K_6 + Hog1} \quad (3)$$

208 where each K_i represents a Michaelis constant, the k_i 's are either the k_{cat} or V_{max} of the reaction,
209 depending on whether the enzyme concentration is explicitly taken into account, and k_b is the
210 basal activation rate (English et al., 2015; Macia et al., 2009). We assumed that salt increases
211 the V_{max} of the reaction for activation of the MAP3K. That is, $k_1 = k_1' KCl$. We used a decreasing
212 Hill function to include negative feedback, with β representing the concentration of active Hog1
213 needed to reduce the MAP3K activation rate by half.

214 Having defined a model, we then sought to fit it to our experimental data. To perform
215 parameter estimation, we created a hybrid method, combining a global and local search method
216 that minimized the distance between simulated fits and the data based on mean squared error
217 (MSE). Recent benchmark efforts have shown that similar combination strategies are
218 particularly efficient and best performing when compared to stand alone methods (Villaverde et
219 al., 2019). Here, we used an evolutionary algorithm (EA) (Fortin et al., 2012) that performs a
220 global search method within a large search space to find best-fitting parameter sets. We then
221 used an approximate Bayesian computation sequential Monte Carlo (ABC SMC) method (Toni
222 et al., 2009) to fine-tune the EA-determined parameter sets to further realize distributions of
223 model parameter values that produced results consistent with the data (Figure 3B-C). This
224 process resulted in 1000 parameter sets that could meet the model-specific MSE thresholds.
225 Details of our parameter optimization method are provided in the Methods section.

226 We fit Model I to our data presented in Figure 2. We simulated wildtype behavior with the
227 full system and simulated kinase-inhibited behavior by removing the Hog1-dependent negative

228 feedback loop. As shown in Figure 3C (top right panel), Model I could neither capture full Hog1
229 activation nor full deactivation. We inferred that Model I was unsuccessful at capturing our data
230 because in the model Hog1 activity immediately suppresses activation of the MAP3K, and
231 consequentially the model cannot simultaneously satisfy the constraints of full activation in
232 wildtype cells and the amplitude dependence of Hog1-as strain. This reasoning is in agreement
233 with work in Schaber et al. 2012 in which they found a delayed negative feedback is necessary
234 for full signal attenuation while negative feedback originating from Hog1 serves to fine-tune the
235 response. Hence, we expanded Model I to include an additional step between Hog1 activation
236 and pathway inhibition to produce a time delay in the negative feedback loop (Figure 3D). This
237 circuitry is consistent with prior models (Ma et al., 2009) and experimental studies, which
238 demonstrate that full HOG pathway adaptation requires an increase in cytosolic osmolytes
239 (Babazadeh et al., 2014; Hohmann, 2002; Siderius et al., 2000), though this model species
240 could represent any upregulated signaling processes downstream of Hog1. Therefore, we
241 updated the model to include this process.

242 *Model II* (Figure 3D):

243 Model I equations 2, and 3 remain the same in Model II. The osmolyte concentration was
244 modeled using the following equation:

$$245 \frac{dOsmolytes}{dt} = s_1 \cdot Hog1 - d_1 \cdot Osmolytes \quad (4)$$

246 where s_1 is the rate of osmolyte synthesis, which requires active Hog1, and d_1 is rate of
247 osmolyte degradation. Model I equation 1 was updated to replace active Hog1 in the negative
248 feedback term with the osmolyte concentration. Overall, adding a delay in the negative feedback
249 loop significantly improved the performance of the model and allowed it to capture full Hog1
250 deactivation (Figure 3 – figure supplement 1). However, Model II still could not capture full Hog1
251 phosphorylation.

252 Investigating the behavior of the osmolyte concentration, we found that Model II
253 predicted a 2-fold increase of the putative osmolyte species over the course of 15 minutes after
254 350 mM KCl stimulus (Figure 3E). To test the model, we exposed cells, with and without Hog1
255 activity, with 350 mM KCl and measured glycerol accumulation over time (Figure 3E). While
256 glycerol exhibited a higher-than predicted increase (four-fold vs two-fold), the dynamics were
257 similar to the model prediction (Figure 3F). The discrepancy in abundance is likely due to Hog1-
258 independent glycerol production. We observed 1- to 2-fold increase of glycerol accumulation in
259 the *hog1Δ* and Hog1-as cells treated with 1-NA-PP1 (Figure 3E, and Figure 3 – figure
260 supplement 2), as reported previously for glycerol and other osmolytes (Babazadeh et al., 2014;
261 Petelenz-Kurdziel et al., 2013; Shellhammer et al., 2017). We then perturbed the behavior of
262 Model II's osmolyte species to understand how the osmolyte concentration controlled Hog1
263 dynamics. Increasing the osmolyte synthesis rate caused the osmolytes to accumulate faster
264 than the fitted simulations which limited Hog1 activation to 5 minutes (Figure 3 – figure
265 supplement 3, left compared to center). Decreasing the osmolyte synthesis rate caused it to
266 accumulate more slowly thereby extending the duration of Hog1 activation to over an hour
267 (Figure 3 – figure supplement 3, left compared to right). This delayed negative feedback does
268 not only control the timing of Hog1 phosphorylation, but also the ability of Hog1 to fully adapt, as
269 seen when decreasing the osmolyte synthesis rate (Figure 3 – figure supplement 3, bottom
270 right). Altogether, these data suggest that a necessary negative feedback originates from a
271 downstream species for full signal attenuation, and that species could likely be the accumulation
272 of intracellular osmolytes.

273 Thus, compared to Model I, Model II was better able to capture Hog1 dose-to duration
274 dynamics and Pbs2 dynamics. However, the revised model still failed to capture full Hog1
275 activation and poorly replicated other features of the data, such as the basal phosphorylation
276 dynamics in the Hog1-as strain. While at this point, we do not rule out Model II from further

277 consideration, its inability to replicate several pathway features motivated us to investigate if
278 other potential feedback loops.

279

280 **Fast positive feedback promotes pathway activation**

281 Model II captured many of the characteristics of Hog1 activation and deactivation.
282 However, Model II did not reach full activation of Hog1, even at the highest concentrations of
283 stimulus. This failure of the model suggests that it lacks an important positive feedback loop.
284 Since Hog1 activation occurs within two minutes, positive feedback would need to act rapidly.
285 Thus, we hypothesized that it originates from Hog1 directly phosphorylating a pathway
286 component. To test this possibility, we expanded Model II into three new models (Models IIa-c)
287 that include Hog1-driven positive feedback loops targeting one of the three kinases in the MAPK
288 kinase cascade: ‘a’ targets the MAP3K, ‘b’ targets Pbs2, and ‘c’ targets Hog1 itself. These
289 loops were modeled by including a term in the relevant activation rate that was proportional to
290 the level of active Hog1.

291 For example, *Model IIc* includes Model II equations 1, 2, 3, and 4 with the following modification
292 to the equation for Hog1:

$$293 \frac{dHog1}{dt} = \frac{(k_5 \cdot Pbs2 + \alpha \cdot Hog1) \cdot Hog1_I}{K_5 + Hog1_I} - \frac{k_6 \cdot Hog1}{K_6 + Hog1} \quad (3)$$

294 where Hog1-mediated positive feedback ($\alpha \cdot Hog1$) increases its own activation.

295 We used the same procedure as described above to train the models. A summary of each
296 model’s fit to the data is provided in Figure 4A. Model IIa produced results very similar to Model
297 II (Figure 4 – figure supplement 1), while Models IIb-c with positive feedback targeting Pbs2 and
298 Hog1, respectively, produced better fits to the data and were able to capture all 10 pathway
299 characteristics (Model IIb: Figure 4 – figure supplement 2, Model IIc: Figure 4B-D). We also
300 found that these two models could predict wildtype Hog1 behavior in response to intermediate
301 single-step KCl concentrations: 250, 350, and 450 mM KCl from in English et al., 2015 (Model

302 IIb: Figure 4 – figure supplement 2, Model IIc: Figure 4E (left)). These models also followed
303 similar Hog1-as dynamics as the previously published though the previously published data is
304 slightly higher than that seen in our data (Figure 4E, right compared to Figure 4D, center). Even
305 with this small discrepancy, these data suggest Hog1 phosphorylates a pathway component at
306 or below that of the MAP2K Pbs2, forming a positive feedback loop.

307 To complete our systematic screen of potential circuitries, we also added positive
308 feedback loops to our Model I to determine whether a positive feedback and direct negative
309 feedback was sufficient to capture our signaling dynamics. Nevertheless, in Models Ia-c, Hog1
310 did not remain fully phosphorylated, diminishing within the first few minutes (Figure 4 – figure
311 supplement 3). Together, these results support the existence of a delayed negative feedback
312 loop as well as a fast positive feedback loop targeting a component within close proximity of
313 Hog1.

314

315 **Experimental validation of computational models reveals positive feedback targeting**
316 **Hog1**

317 A successful model must not only fit relevant data but also predict new behavior. One
318 particularly informative approach is to use such models to predict the response to dynamic input
319 and determine whether they are able to capture dynamics more complex than those used to
320 train the model. With two pathway circuitries (Models IIb and IIc) that sufficiently captured our
321 data (Figure 5A), we aimed to differentiate them by predicting Hog1 behavior in response to
322 increasing step stimuli. To identify the best model, we sought an input that produced different
323 outputs for each model, and to then test those conditions experimentally (Mélykúti et al., 2010).

324 Following this strategy, we computationally generated 1000 random input profiles of
325 increasing salt concentrations and predicted Hog1 response to each input profile using Models
326 IIb and IIc. These step profiles were designed so that they could be experimentally tested in
327 vivo. We ranked the resulting input profiles based on which generated the largest differences in

328 the Hog1 response (Figure 5B). For example, Figure 5C shows three selected inputs ("Step")
329 that correspond to the Hog1 dynamics predicted by the two models in Figure 5D. Step #100
330 generated similar predictions among the models while Step #990 resulted in distinct Hog1
331 behaviors. Step #550 also predicted model-dependent dynamics, but the differences were too
332 small to be experimentally decipherable. Generally, the input profiles that produced the greatest
333 difference between the Hog1 behaviors were those that allowed Hog1 to adapt to an initial step
334 of KCl before introducing a second step (shaded area in Figure 5B). For Step #990, Model IIb
335 predicted that Hog1 would show a diminished response to the second step of stimulus, but
336 Model IIc predicted full Hog1 phosphorylation in response to this second step (Figure 5D right
337 column). These results indicated that Step #990 would discriminate between the two models.

338 We then measured the biological Hog1 response to Step #990. We exposed cells to the
339 stimulus profile used in our simulations: beginning with an initial salt stimulus of 250 mM KCl
340 and then raising the salt concentration to 550 mM KCl after 20 minutes. Hog1 activity was again
341 measured by Phos-tag immunoblotting (Figure 5E, left). Quantitation of the blots shows that
342 Hog1 responded normally to the first step of stimulus – becoming completely phosphorylated by
343 two minutes and then fully adapting within 15 minutes (Figure 5E, right). Upon the second
344 stimulus step, Hog1 was again fully activated and then fully adapted. This result was similar to
345 previously published measures of Hog1 translocation and phosphorylation (by phospho-p38
346 immunoblotting) in response to steps of equal magnitude (Behar et al., 2007; Hao et al., 2007;
347 Zi et al., 2010). In further support of Model IIc, we then predicted Hog1 dual phosphorylation if
348 its kinase activity was inhibited directly before the second stimulus step of Step #990. To
349 conduct this experiment, we utilized the Hog1-as strain. Again, results most closely aligned with
350 Model IIc (Figure 5 – figure supplement 1). Thus, our experimental results to Step #990, both
351 with and without kinase activity, most closely aligned to the predicted Hog1 dynamics of Model
352 IIc, indicating that positive feedback likely acts at the level of Hog1 rather than elsewhere in the
353 MAPK cascade.

354

355 **Positive feedback is independent of feedback phosphorylation**

356 Our modeling results suggested that positive feedback amplifies the signal at the level of
357 Hog1. There are two ways in which feedback phosphorylation could activate the MAPK:
358 increase its phosphorylation rate (Figure 6) or decrease its dephosphorylation rate (Figure 7).
359 Since positive feedback must happen quickly, it seemed likely that the target of feedback
360 regulation is a direct substrate of Hog1. Hog1, like all MAPKs, phosphorylates proteins at a
361 serine or threonine followed by a proline. Phosphorylation at these sites typically invokes
362 conformational changes or alters binding affinities, resulting in rapid changes in substrate
363 function (Humphrey et al., 2015; Ubersax and Ferrell, 2007). If positive feedback is due to
364 phosphorylation by Hog1, then mutating the MAPK consensus sites in potential feedback
365 targets should dampen Hog1 activity.

366 We then used Model IIc to investigate how feedback phosphorylation could amplify Hog1
367 phosphorylation. By assigning the activation rate α to 0, thereby eliminating positive feedback,
368 the model predicted a reduction in Hog1 phosphorylation, particularly at low salt concentrations
369 (Figure 6B). Based on these predictions, we anticipated that 350 mM KCl would be particularly
370 informative since it was low enough to cause at least a 25% decrease in Hog1 phosphorylation
371 over several timepoints (Figure 6B). To disrupt the putative positive feedback loop, we mutated
372 the two MAPK consensus sites on Hog1 ($Hog1^{2A}$ mutant) and monitored its phosphorylation in
373 response to 350 mM KCl. Immunoblotting after Phos-tag SDS-PAGE showed that these
374 mutations did not alter Hog1 dynamics (Figure 6C), in contrast to predictions of Model IIc. We
375 then considered Pbs2 as a potential substrate since it is responsible for Hog1 activation. We
376 mutated its 6 MAPK consensus sites ($Pbs2^{6A}$ mutant), and found that these alterations also
377 produced minimal changes in Hog1 activation (Figure 6D). Taken together, these results
378 suggest that phosphorylation of Pbs2 or Hog1 is not the source of positive feedback in the
379 system.

380

381 **Positive feedback results from mutual inhibition of Hog1 and its phosphatases**

382 We then considered an alternative scenario where Hog1 acts by decreasing its own rate
383 of deactivation. In practice, this could be achieved by Hog1 inhibition of its phosphatases. We
384 constructed a new model, Model III, that incorporated another model species representing Hog1
385 phosphatases and included mutual inhibition between the phosphatases and Hog1.

386 *Model III:*

387 consisted of Model II's equations 1, 2, 3, and 4 with the following modifications:

$$388 \frac{dHog1}{dt} = \frac{k_5 \cdot Pbs2 \cdot Hog1_I}{K_5 + Hog1_I} - \frac{(k_6 + \alpha_1 \cdot Phosphatase) \cdot Hog1}{K_6 + Hog1} \quad (3)$$

$$389 \frac{dPhosphatase}{dt} = \frac{k_7 \cdot Phosphatase_I}{K_7 + Phosphatase_I} - \frac{(k_8 + \alpha_2 \cdot Hog1) \cdot Phosphatase}{K_8 + Phosphatase} \quad (5)$$

390 where α_1 is phosphatase-driven Hog1 suppression and α_2 is Hog1-driven phosphatase
391 suppression. Here, the total phosphatase concentration is conserved.

392 We determined whether Model III could perform equal to or outperform Model IIc. We
393 trained Model III on the same phosphorylation data for both Pbs2 and Hog1, as previously done
394 for Model IIc (Figure 3). Resulting fits to Model III captured our 10 pathway characteristics as
395 well as Model IIc (Figure 7 – figure supplement 1). Based on these results, we conclude that
396 mutual inhibition is a candidate for positive feedback in HOG signaling pathway.

397 Next, we sought to gain experimental evidence in support of our mutual inhibition
398 hypothesis. We examined three potential targets of mutual inhibition: the Hog1-directed
399 phosphatases Ptc1, Ptp2, and Ptp3 (Jacoby et al., 1997; Mattison and Ota, 2000; Warmka et
400 al., 2001; Wurgler-Murphy et al., 1997). Ptc1 dephosphorylates Hog1 at its activation loop
401 threonine site while Ptp2 and Ptp3 dephosphorylate the remaining tyrosine site. Among these
402 three phosphatases there are 22 putative MAPK consensus sites. Hog1 could phosphorylate a
403 combination of these sites to suppress phosphatase activity. Since mutating every site was

404 infeasible, we instead deleted the *PTC1*, *PTP2*, *PTP3* genes and monitored Hog1
405 phosphorylation. Each deletion caused mild changes to the timing of Hog1 dephosphorylation,
406 but did not result in the partial Hog1 activation that the model predicted (Figure 7 – figure
407 supplement 2). This result suggests that a single phosphatase is unlikely to be responsible for
408 feedback regulation.

409 Existing evidence indicates that the three phosphatases work together to regulate Hog1,
410 making it likely that Hog1, in turn, inhibits multiple phosphatases. In particular, dual deletions of
411 *PTC1* and *PTP2* are lethal, most likely due to Hog1 hyperactivation (Maeda et al., 1993). Our
412 previously published data showed that Hog1 was basally phosphorylated in a *ptp2Δptp3Δ*
413 background (English et al., 2015). Additional investigation revealed that deletion of both *PTP2*
414 and *PTP3* results in high (70%) basal phosphorylation of Hog1 (Figure 7A); in response to 350
415 mM KCl, Hog1 is fully phosphorylated and then returns back to 70% basal activation. Though
416 this experimental result alone is insufficient to suggest that positive feedback acts through
417 mutual inhibition, we could nevertheless use this data to retrain our models to determine if
418 positive feedback was needed in the system.

419 To distinguish between the mutual inhibition and positive feedback loop mechanisms, we
420 compared how well Model III and IIc fit our *ptp2Δptp3Δ* data. If this mutual inhibition applied,
421 Model III should be able to capture all of the phosphorylation data, indicating that positive
422 feedback is not present within a *ptp2Δptp3Δ* background. In contrast, should Model IIc capture
423 this data, this would imply positive feedback is still present within a *ptp2Δptp3Δ* background,
424 since we are only eliminating phosphatase suppression of Hog1 activity but not the positive
425 feedback loop. Thus, we retrained Model IIc and III to the basal phosphorylation of the
426 *ptp2Δptp3Δ* data and compared their performance. For Model IIc, we simulated *ptp2Δptp3Δ* by
427 fitting a separate Hog1 deactivation rate. For Model III, we simulated phosphatase deletion by
428 setting their concentration to 0 (Figure 7B). Fitting to these additional data, we found that Model
429 III was able to capture the experimental data (Figure 7C, top) whereas Model IIc could not,

430 particularly in the wildtype strain (Figure 7C, bottom). Model III could also correctly predict the
431 Hog1 response to Step #990 (Figure 7D, top right) and nearly predicted the behavior of the
432 *ptp2Δptp3Δ* strain to a single step of 350 mM KCl (Figure 7D, top left). The only discrepancy
433 between Model III and the experimental result was that the experimental measurements for the
434 *ptp2Δptp3Δ* strain showed faster adaptation than predicted in our simulations. However, this
435 faster dephosphorylation is likely driven by other yeast phosphatases not present in the model.
436 Meanwhile, the retrained Model IIc poorly predicted the Hog1 dynamics in response to 350 mM
437 KCl (Figure 7D, bottom left) and the full Hog1 phosphorylation in response to Step #990 (Figure
438 7D, bottom right). The performance of Model III, in both its fits to the data and its prediction of
439 the increasing step stimulus behavior, provides strong evidence for mutual inhibition between
440 Hog1 and its phosphatases. We conclude that mutual inhibition is responsible for positive
441 feedback in the HOG MAPK cascade.

442

443 Discussion

444 Feedback regulation often controls the timing of signaling events, allowing for an
445 appropriate cellular response. For the HOG pathway, we and others have previously shown that
446 a progressively stronger input leads to a progressively longer output (Aymoz et al., 2016; Behar
447 et al., 2008; English et al., 2015). What has been lacking is a comprehensive understanding of
448 the feedback mechanisms responsible for the encoding of this distinctive “dose-to-duration”
449 signaling profile. To elucidate these mechanisms, we systematically tested 8 network
450 architectures and found two that could fit our experimental data. By changing the input profile
451 and predicting Hog1 response, we found conditions that could differentiate between the two
452 models. Experimental validation identified slow negative feedback and fast positive feedback as
453 the most likely circuitry. We then tested potential mechanisms of positive feedback, with our
454 data suggesting positive feedback acts through mutual inhibition between Hog1 and the tyrosine

455 phosphatases, Ptp2 and Ptp3. Thus, our iterative approach allowed us to identify new
456 mechanisms of regulation in the canonical HOG pathway.

457 Our findings build on other investigations of feedback within the HOG pathway. Our own
458 previous models incorporated positive feedback, but did not explore how positive feedback acts
459 in conjunction with negative feedback to control Hog1 activation dynamics (English et al., 2015).
460 The present work highlights the importance of tyrosine phosphatases together with osmolyte
461 accumulation. However, other feedback mechanisms are likely to be important for controlling
462 Hog1 dynamics. These could include known mechanisms, such as Hog1 phosphorylation of
463 upstream components and other Hog1-directed phosphatases. Other mechanisms of feedback
464 have been suggested, particularly between the two input branches which seem to suppress one
465 another's activity (Granados et al., 2017). Thus, feedback likely acts on a variety of components
466 to continuously fine-tune the cell's response to a given stimulus. Looking forward, investigating
467 the response of Hog1 to even more complex inputs, including different ramps (Thiemicke et al.,
468 2019) or pulses, will further clarify the roles of individual feedbacks within the system.

469 More generally, the results provided here suggest that the counter-acting mechanisms of
470 positive and negative feedback determine the prioritization of intracellular events following
471 hyperosmotic stress. These events are likely to occur on various timescales. For example,
472 shortly after the stimulus, Hog1 phosphorylates a regulator of Fps1, a glycerol export channel,
473 resulting in rapid channel closure and the accumulation of glycerol in the cell (Lee et al., 2013).
474 On a longer timescale, Hog1 phosphorylates transcription factors resulting in new gene
475 expression (Alepuz et al., 2001; Capaldi et al., 2008). With prolonged stimulation, Hog1
476 activates multiple transcription factors and in so doing employs additional regulatory
477 mechanisms such as feedforward loops (AkhavanAghdam et al., 2016). The timing of these
478 actions suggests a prioritized order of intracellular events, presumably to enhance a cell's
479 chance of surviving hyperosmotic stresses.

480 Collectively, these efforts illustrate how computational modeling allows us to probe
481 behaviors that are difficult to predict or explain through experimentation alone. When models
482 are based on quantitative data and describe well-defined molecular networks, it is possible to
483 extract information about the system and make predictions of how that system behaves under
484 complex situations. Here we found step stimuli that could differentiate the predicted behaviors of
485 models that captured our experimental data. This model-driven experimental design not only
486 provided insights into circuit-specific behaviors, but it also revealed putative mechanisms of
487 positive feedback.

488 Likewise, insights developed from the yeast system could reveal regulatory roles of other
489 MAPKs in more complex systems. In a broader context, understanding how pathways control
490 MAPK regulation is critical for pharmaceutical development. Protein kinases are the second
491 largest group of drug targets, and are particularly important in the treatment of cancers.
492 Moreover, one of the main challenges of drug development is overcoming kinase inhibitor
493 resistance within complex pathway systems (Bhullar et al., 2018). Understanding the
494 mechanisms of spatiotemporal pathway regulation will ultimately lead to the development of
495 novel techniques to control kinase activity.

496

497 **Materials and Methods**

498 **Strain construction and plasmids**

499 Strains (Table 1) were derived from BY4741 (“wildtype”) and transformed by the lithium acetate
500 method (Gietz and Woods, 2002). Pbs2-9xMyc-tagged strains were generated by homologous
501 recombination of a PCR-amplified 9xMyc cassette at the C-terminus of the *PBS2* open reading
502 frame. This cassette contained a resistance gene to hygromycin from plasmid pYM20-
503 9xMyc-hphNT1) (Janke et al., 2004).

504 Mutagenesis for Hog1 (S91A and S235A) and Pbs2 (S83A, T164A, T212, S248A,
505 T297A, and S415A) were introduced using the *delitto perfetto* method (Stuckey et al., 2011)
506 using the PCR-amplified pCORE cassette (RRID:Addgene_72231) to integrate selective
507 markers at the endogenous gene loci. These markers were selected against after the integration
508 of synthesized gBlocks (Integrated DNA Technologies). All strains were validated with PCR, and
509 mutated genes were PCR-amplified and sequenced.

510 Table 1

Strain	Genotype	Background	Reference
BY4741	<i>MATa, his3Δ1, leu2Δ, met15Δ, ura3Δ</i>	BY4743	(Brachmann et al., 1998)
SKS001	<i>HOG1^{T100A}</i>	BY4741	(English et al., 2015)
SKS002	Pbs2-9xMyc:: <i>hphNT1</i>	BY4741	This study
SKS003	<i>HOG1^{T100A}</i> Pbs2-9xMyc:: <i>hphNT1</i>	SKS001	This study
SKS004	<i>PBS2^{6A}</i>	BY4741	This study
SKS005	<i>HOG1^{2A}</i>	BY4741	This study
SKS006	<i>ptp2Δ::URA3</i>	BY4741	(English et al., 2015)
SKS007	<i>ptp3Δ::KanMX4</i>	BY4741	(English et al., 2015)
SKS008	<i>ptc1Δ::KanMX4</i>	BY4741	(English et al., 2015)
SKS009	<i>ptp2Δ::URA3</i> <i>ptp3Δ::KanMX4</i>	SKS006	This study

511

512

513 **Cell culture**

514 Strains were cultured using standard methods and media. Strains were struck out on YPD
515 (yeast extract, peptone, and 2% dextrose) plates and cultured at 30°C. Individual colonies were
516 picked and grown overnight in 3 mLs SCD (synthetic complete and 2% dextrose) medium to
517 saturation. Cells were diluted 1:100, grown for 8 hours, and diluted to OD₆₀₀ = 0.001 for
518 overnight growth. The following day, experiments were conducted once the cell culture reached
519 an OD₆₀₀ ~1.

520

521 **Phos-tag sample collection, gel electrophoresis, and immunoblotting**

522 Kinase activation was quantified using Phos-tag immunoblotting technique as previously
523 described (English et al., 2015). Briefly, cells were cultured with a final volume of 80 mLs in
524 SCD. For Hog1-as (Hog1^{T100A} + 1-NA-PP1) kinase inhibition, 1-NA-PP1 ATP analog (Cayman
525 Chemical, #10954) was added to cultures to a final concentration of 12 µM and incubated for 2
526 min before sampling. At the selected timepoints after the addition of KCl in SCD, samples were
527 quenched in 5% (v/v) trichloroacetic acid (TCA) on ice, washed with 5% sodium azide, and
528 stored at -80°C. Sample concentrations were normalized to 1.5 µg/µL using the DC Protein
529 Assay (Bio-Rad) and stored at -80°C.

530 Samples were resolved using 8% acrylamide 20 uM Phos-tag Bis-Tris SDS-PAGE gels
531 and transferred on to PVDF membrane. Hog1 was detected using an anti-Hog1 primary-
532 antibody (Santa Cruz, Hog1 antibody (D-3) sc-165978; 1:5,000) and a donkey-anti mouse HRP-
533 conjugated secondary antibody (Jackson ImmunoResearch, 715-035-150; 1:10,000). Pbs2-
534 9xMyc was detected using an anti-Myc primary antibody (Cell Signaling, 9B11 #2276, 1:5,000)
535 and a donkey anti-rabbit HRP-conjugated secondary antibody (Jackson ImmunoResearch, 711-
536 035-152; 1:10,000). Secondary antibodies were visualized using Clarity Western ECL Substrate
537 (Bio-Rad, #1705061) and a BioRad Chemidoc Touch Imaging System. Band intensities were
538 normalized and quantified using the ImageLab (Bio-Rad) software. We found that additional
539 bands were occasionally observed, that would vary between technical replicates, indicating that

540 their existence was due to gel and immunoblotting inconsistencies rather than being other
541 phospho-states of Hog1. Also, band migration depended on the number of gels run
542 simultaneously. Standard error of the mean was plotted since models were fit to mean values.

543

544 **Glycerol measurements**

545 Samples of 1 mL were collected at the selected timepoints after the addition of KCl in SCD and
546 kinase inhibition, when applicable, as above. 500 µL was used to measure OD₆₀₀ and the
547 remaining 500 µL was pelleted and frozen in liquid nitrogen. After collection, samples were
548 boiled for 10 min in sterile water and cleared by centrifugation. The concentration of glycerol
549 was measured using a Free Glycerol Assay Kit (abcam, ab65337) following the manufacturing
550 instructions. Conversion between OD₆₀₀ and cell number was calculated by counting the cells
551 growing in liquid culture with a hemocytometer and measuring the OD₆₀₀ simultaneously (n = 3).
552 These measurements were fit using logarithmic function, which served as a standard curve for
553 our sample measurements to calculate cell number.

554

555 **ODE modeling and parameter optimization**

556 Modeling was performed in Python 3.7 using the scipy package to solve ODE systems and their
557 steady states. All kinases and phosphatases observed mass conservation with the total protein
558 amounts reflecting biologically observed concentrations (Ho et al., 2018). These models rely on
559 different assumptions. First, we do not include synthesis or degradation of the kinases because
560 hyperosmotic stress does not induce their transcription (O'Rourke and Herskowitz, 2004) and
561 quantification of Hog1 and Pbs2 time course immunoblots indicates that protein concentration
562 does not change appreciably throughout our experiments (data not shown). Furthermore, we
563 group the three HOG pathway MAP3Ks into one species, assuming that they share the same
564 kinetic behavior. We reason that we are studying the overall behavior of Pbs2 and Hog1, which
565 are downstream of the two input branches.

566 For parameter optimization, we combined two approaches that have been used to
567 parameterize ODE models to experimental data: an evolutionary algorithm (EA) (Fortin et al.,
568 2012) and an approximate Bayesian Computation and sequential Monte Carlo (ABC SMC)
569 (Toni et al., 2009). All values for k_{cat} , K_M , synthesis, degradation, and feedback terms needed to
570 be estimated to fit each model to our experimental data.

571 First, the EA seeded each simulation with starting values that were randomly selected
572 from a user specified range. Then, the EA would evaluate the fits of each parameter set to the
573 experimental data using MSE and select the best fitting parameter sets to continue to the next
574 generation. To avoid local optima, each parameter set has a 10% probability to crossover with
575 another set, and each parameter has a 20% probability to mutate to a different value. For each
576 model, we calculated the fit of 500 parameter sets over 1000 generations for 2000 independent
577 runs. For each run, we saved the top fitting parameter set. We noticed that it was difficult to
578 programmatically separate out the top fitting parameter sets: when we ranked the MSEs, there
579 was a sharp increase in MSEs, then a gradual increase, followed by another sharp increase.
580 Where these transitions occurred varied with each model, and their resulting fits to the data also
581 depended on the model.

582 Thus, we chose to use the best (lowest-scoring) 500 EA parameters vectors from the EA
583 as priors for the ABC SMC to further sample for the optimal parameters of each model. This
584 loose inclusion of the best 25% parameter sets allowed the ABC SMC to further search the
585 parameter space in case the EA missed any optima. We then followed the same algorithm as in
586 Toni 2009 in which sampled parameter vectors must pass a series of tolerance levels (ϵ)
587 determined by their fit to the experimental data, where the first tolerance was the worst MSE of
588 the top 25% EA parameter sets and all subsequent tolerances were the average of the previous
589 tolerance and the best MSE from the top 25% EA parameter sets. For each model, we ran four
590 series, or “schedules,” in which each schedule included 1000 parameter vectors that passed its
591 tolerance. During a schedule, a parameter vector was selected based on its importance weight

592 and perturbed. This weight is calculated by the prior and the perturbation of each parameter.
593 We used a perturbation kernel of U(-1,1) around \log_{10} transformed parameter values so that
594 sampling was scaled to the magnitude of the value. Since all priors and perturbation kernels for
595 these simulations were uniform, each parameter set had an equal probability of being selected.
596 After each schedule, we calculated new weights for the selected parameter values. In the end,
597 we had 1000 parameter vectors that passed the highest tolerance threshold.

598

599 All simulations and analysis were performed using custom scripts which are available at
600 https://github.com/sksuzuki/HOG_encoding_feedbacks.

601

602 **Model differentiation**

603 Once we found two models that could capture our experimental data, we needed to identify the
604 most likely circuitry of the two. We generated increasing step stimuli and simulated Hog1
605 response with each model. Each stimulus was randomly generated, but we limited them to three
606 rules. First, the stimulus must always increase because decreasing osmolarity would activate a
607 hypoosmotic response. While the Sln1 branch contributes to the hypoosmotic response, there
608 are other mechanisms outside of the HOG pathway that control yeast response to hypoosmotic
609 stress (Brown et al., 1994). Second, we limited the increasing steps to a maximal stimulus of
610 550 mM KCl due to increased cell death above this concentration. Third, we limited the intervals
611 of each step to at least 2 minutes since faster intervals are not experimentally feasible.
612 Generated inputs were then ranked based on maximizing the distance between model
613 predictions. Thus, the larger distance reflected the greatest difference between the simulated
614 Hog1 dynamics.

615

616 **Author Contributions**

617 SKS, BE, HGD, and TCE were responsible for conceptualization. SKS, HGD, and TCE
618 designed experiments. SKS constructed strains and performed experiments, data analysis, and
619 mathematical modeling. SKS created visualizations. SKS, HGD, and TCE were responsible for
620 writing with review assistance from BE.

621

622 **Acknowledgments**

623 We thank Jeremy Purvis, Joel Parker, Michael Pablo, and Amy Pomeroy for helpful discussion,
624 James Shellhammer for guidance on the experimental procedures, Jeff Snell for assistance in
625 developing the evolutionary algorithm, Rozemarijn van der Veen for editing the manuscript, and
626 Joseph McGirr for feedback. This work was supported by the National Institutes of Health (NIH)
627 training grant T32 GM067553-12 (SKS), the NIH Maximizing Investigators' Research Award
628 (MIRA) R35 GM127145 (TCE), and the NIH MIRA R35 GM118105 (HGD).

629

630

631

632

633

634

635

636

637

638

639

- 640 AkhavanAghdam, Z., Sinha, J., Tabbaa, O.P., Hao, N., 2016. Dynamic control of gene
641 regulatory logic by seemingly redundant transcription factors. *Elife* 5.
642 doi:10.7554/eLife.18458
- 643 Albeck, J.G., Mills, G.B., Brugge, J.S., 2013. Frequency-modulated pulses of ERK activity
644 transmit quantitative proliferation signals. *Mol. Cell* 49, 249–261.
645 doi:10.1016/j.molcel.2012.11.002
- 646 Alepuz, P.M., Jovanovic, A., Reiser, V., Ammerer, G., 2001. Stress-induced map kinase Hog1 is
647 part of transcription activation complexes. *Mol. Cell* 7, 767–777. doi:10.1016/s1097-
648 2765(01)00221-0
- 649 Alon, U., 2007. Network motifs: theory and experimental approaches. *Nat. Rev. Genet.* 8, 450–
650 461. doi:10.1038/nrg2102
- 651 Aymoz, D., Wosika, V., Durandau, E., Pelet, S., 2016. Real-time quantification of protein
652 expression at the single-cell level via dynamic protein synthesis translocation reporters.
653 *Nat. Commun.* 7, 11304. doi:10.1038/ncomms11304
- 654 Babazadeh, R., Furukawa, T., Hohmann, S., Furukawa, K., 2014. Rewiring yeast osmostress
655 signalling through the MAPK network reveals essential and non-essential roles of Hog1
656 in osmoadaptation. *Sci. Rep.* 4, 4697. doi:10.1038/srep04697
- 657 Behar, M., Hao, N., Dohlman, H.G., Elston, T.C., 2007. Mathematical and computational
658 analysis of adaptation via feedback inhibition in signal transduction pathways. *Biophys.
659 J.* 93, 806–821. doi:10.1529/biophysj.107.107516
- 660 Behar, M., Hao, N., Dohlman, H.G., Elston, T.C., 2008. Dose-to-duration encoding and signaling
661 beyond saturation in intracellular signaling networks. *PLoS Comput. Biol.* 4, e1000197.
662 doi:10.1371/journal.pcbi.1000197
- 663 Bhullar, K.S., Lagarón, N.O., McGowan, E.M., Parmar, I., Jha, A., Hubbard, B.P., Rupasinghe,
664 H.P.V., 2018. Kinase-targeted cancer therapies: progress, challenges and future
665 directions. *Mol. Cancer* 17, 48. doi:10.1186/s12943-018-0804-2
- 666 Brachmann, C.B., Davies, A., Cost, G.J., Caputo, E., Li, J., Hieter, P., Boeke, J.D., 1998.
667 Designer deletion strains derived from *Saccharomyces cerevisiae* S288C: a useful set of
668 strains and plasmids for PCR-mediated gene disruption and other applications. *Yeast*
669 14, 115–132. doi:10.1002/(SICI)1097-0061(19980130)14:2<115::AID-
670 YEA204>3.0.CO;2-2
- 671 Brandman, O., Meyer, T., 2008. Feedback loops shape cellular signals in space and time.
672 *Science* 322, 390–395. doi:10.1126/science.1160617
- 673 Brewster, J.L., Gustin, M.C., 2014. Hog1: 20 years of discovery and impact. *Sci. Signal.* 7, re7.
674 doi:10.1126/scisignal.2005458
- 675 Brown, J.L., Bussey, H., Stewart, R.C., 1994. Yeast Skn7p functions in a eukaryotic two-
676 component regulatory pathway. *EMBO J.* 13, 5186–5194. doi:10.1002/j.1460-
677 2075.1994.tb06849.x

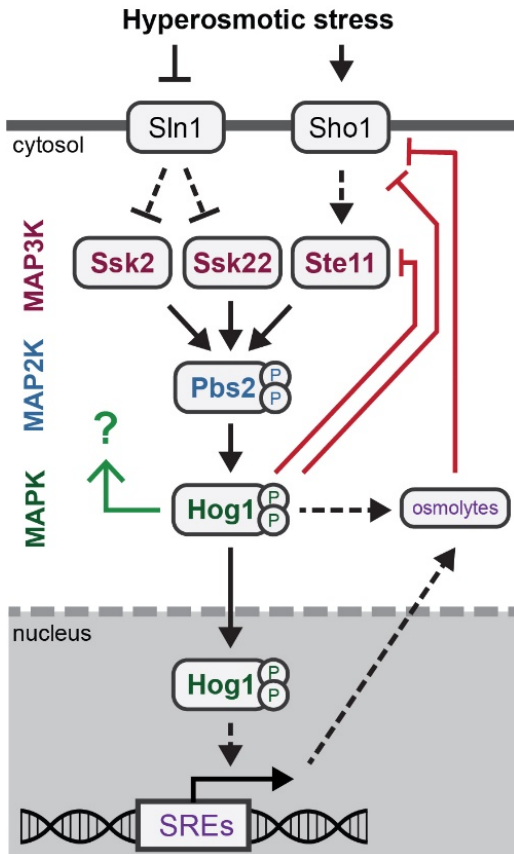
- 678 Capaldi, A.P., Kaplan, T., Liu, Y., Habib, N., Regev, A., Friedman, N., O'Shea, E.K., 2008.
679 Structure and function of a transcriptional network activated by the MAPK Hog1. *Nat.*
680 *Genet.* 40, 1300–1306. doi:10.1038/ng.235
- 681 Cargnello, M., Roux, P.P., 2011. Activation and function of the MAPKs and their substrates, the
682 MAPK-activated protein kinases. *Microbiol. Mol. Biol. Rev.* 75, 50–83.
683 doi:10.1128/MMBR.00031-10
- 684 English, J.G., Shellhammer, J.P., Malahe, M., McCarter, P.C., Elston, T.C., Dohlman, H.G.,
685 2015. MAPK feedback encodes a switch and timer for tunable stress adaptation in yeast.
686 *Sci. Signal.* 8, ra5. doi:10.1126/scisignal.2005774
- 687 Escoté, X., Miranda, M., Rodríguez-Porrata, B., Mas, A., Cordero, R., Posas, F., Vendrell, J.,
688 2011. The stress-activated protein kinase Hog1 develops a critical role after resting
689 state. *Mol. Microbiol.* 80, 423–435. doi:10.1111/j.1365-2958.2011.07585.x
- 690 Ferrell, J.E., 2016. Perfect and Near-Perfect Adaptation in Cell Signaling. *Cell Syst.* 2, 62–67.
691 doi:10.1016/j.cels.2016.02.006
- 692 Fortin, F.-A., De Rainville, F.-M., Gardner, M.-A., Parizeau, M., Gagné, C., 2012. DEAP:
693 Evolutionary Algorithms Made Easy François-Michel De Rainville. *Journal of Machine*
694 *Learning Research* 13, 2171–2175.
- 695 Gietz, R.D., Woods, R.A., 2002. Transformation of yeast by lithium acetate/single-stranded
696 carrier DNA/polyethylene glycol method. *Meth. Enzymol.* 350, 87–96.
- 697 Granados, A.A., Crane, M.M., Montano-Gutierrez, L.F., Tanaka, R.J., Voliotis, M., Swain, P.S.,
698 2017. Distributing tasks via multiple input pathways increases cellular survival in stress.
699 *eLife* 6. doi:10.7554/eLife.21415
- 700 Hao, N., Behar, M., Parnell, S.C., Torres, M.P., Borchers, C.H., Elston, T.C., Dohlman, H.G.,
701 2007. A systems-biology analysis of feedback inhibition in the Sho1 osmotic-stress-
702 response pathway. *Curr. Biol.* 17, 659–667. doi:10.1016/j.cub.2007.02.044
- 703 Hersen, P., McClean, M.N., Mahadevan, L., Ramanathan, S., 2008. Signal processing by the
704 HOG MAP kinase pathway. *Proc. Natl. Acad. Sci. USA* 105, 7165–7170.
705 doi:10.1073/pnas.0710770105
- 706 Ho, B., Baryshnikova, A., Brown, G.W., 2018. Unification of Protein Abundance Datasets Yields
707 a Quantitative *Saccharomyces cerevisiae* Proteome. *Cell Syst.* 6, 192–205.e3.
708 doi:10.1016/j.cels.2017.12.004
- 709 Hohmann, S., 2002. Osmotic stress signaling and osmoadaptation in yeasts. *Microbiol. Mol.*
710 *Biol. Rev.* 66, 300–372. doi:10.1128/mmbr.66.2.300-372.2002
- 711 Humphrey, S.J., James, D.E., Mann, M., 2015. Protein phosphorylation: A major switch
712 mechanism for metabolic regulation. *Trends Endocrinol. Metab.* 26, 676–687.
713 doi:10.1016/j.tem.2015.09.013
- 714 Jacoby, T., Flanagan, H., Faykin, A., Seto, A.G., Mattison, C., Ota, I., 1997. Two protein-
715 tyrosine phosphatases inactivate the osmotic stress response pathway in yeast by

- 716 targeting the mitogen-activated protein kinase, Hog1. *J. Biol. Chem.* 272, 17749–17755.
717 doi:10.1074/jbc.272.28.17749
- 718 Janke, C., Magiera, M.M., Rathfelder, N., Taxis, C., Reber, S., Maekawa, H., Moreno-Borchart,
719 A., Doenges, G., Schwob, E., Schiebel, E., Knop, M., 2004. A versatile toolbox for PCR-
720 based tagging of yeast genes: new fluorescent proteins, more markers and promoter
721 substitution cassettes. *Yeast* 21, 947–962. doi:10.1002/yea.1142
- 722 Janschitz, M., Romanov, N., Varnavides, G., Hollenstein, D.M., Gérecová, G., Ammerer, G.,
723 Hartl, M., Reiter, W., 2019. Novel interconnections of HOG signaling revealed by
724 combined use of two proteomic software packages. *Cell Commun. Signal.* 17, 66.
725 doi:10.1186/s12964-019-0381-z
- 726 Kinoshita, E., Kinoshita-Kikuta, E., Takiyama, K., Koike, T., 2006. Phosphate-binding tag, a new
727 tool to visualize phosphorylated proteins. *Mol. Cell Proteomics* 5, 749–757.
728 doi:10.1074/mcp.T500024-MCP200
- 729 Klein, M., Morillas, M., Vendrell, A., Brive, L., Gebbia, M., Wallace, I.M., Giaever, G., Nislow, C.,
730 Posas, F., Grøtli, M., 2011. Design, synthesis and characterization of a highly effective
731 inhibitor for analog-sensitive (as) kinases. *PLoS One* 6, e20789.
732 doi:10.1371/journal.pone.0020789
- 733 Klipp, E., Nordlander, B., Krüger, R., Gennemark, P., Hohmann, S., 2005. Integrative model of
734 the response of yeast to osmotic shock. *Nat. Biotechnol.* 23, 975–982.
735 doi:10.1038/nbt1114
- 736 Klipp, E., Schaber, J., 2008. Modeling the dynamics of stress activated protein kinases (SAPK)
737 in cellular stress response, in: Posas, F., Nebreda, A.R. (Eds.), *Stress-Activated Protein*
738 *Kinases*. Springer Berlin Heidelberg, Berlin, Heidelberg, pp. 205–224.
739 doi:10.1007/4735_2007_0241
- 740 Kung, C., Kenski, D.M., Krukenberg, K., Madhani, H.D., Shokat, K.M., 2006. Selective kinase
741 inhibition by exploiting differential pathway sensitivity. *Chem. Biol.* 13, 399–407.
742 doi:10.1016/j.chembiol.2006.02.004
- 743 Lee, J., Reiter, W., Dohnal, I., Gregori, C., Beese-Sims, S., Kuchler, K., Ammerer, G., Levin,
744 D.E., 2013. MAPK Hog1 closes the *S. cerevisiae* glycerol channel Fps1 by
745 phosphorylating and displacing its positive regulators. *Genes Dev.* 27, 2590–2601.
746 doi:10.1101/gad.229310.113
- 747 Ma, W., Trusina, A., El-Samad, H., Lim, W.A., Tang, C., 2009. Defining network topologies that
748 can achieve biochemical adaptation. *Cell* 138, 760–773. doi:10.1016/j.cell.2009.06.013
- 749 Macia, J., Regot, S., Peeters, T., Conde, N., Solé, R., Posas, F., 2009. Dynamic signaling in the
750 Hog1 MAPK pathway relies on high basal signal transduction. *Sci. Signal.* 2, ra13.
751 doi:10.1126/scisignal.2000056
- 752 Maeda, T., Tsai, A.Y., Saito, H., 1993. Mutations in a protein tyrosine phosphatase gene (PTP2)
753 and a protein serine/threonine phosphatase gene (PTC1) cause a synthetic growth
754 defect in *Saccharomyces cerevisiae*. *Mol. Cell. Biol.* 13, 5408–5417.
755 doi:10.1128/mcb.13.9.5408

- 756 Mattison, C.P., Ota, I.M., 2000. Two protein tyrosine phosphatases, Ptp2 and Ptp3, modulate
757 the subcellular localization of the Hog1 MAP kinase in yeast. *Genes Dev.* 14, 1229–
758 1235.
- 759 Mélykúti, B., August, E., Papachristodoulou, A., El-Samad, H., 2010. Discriminating between
760 rival biochemical network models: three approaches to optimal experiment design. *BMC*
761 *Syst. Biol.* 4, 38. doi:10.1186/1752-0509-4-38
- 762 Mettetal, J.T., Muzzey, D., Gómez-Uribe, C., van Oudenaarden, A., 2008. The frequency
763 dependence of osmo-adaptation in *Saccharomyces cerevisiae*. *Science* 319, 482–484.
764 doi:10.1126/science.1151582
- 765 Miermont, A., Uhlendorf, J., McClean, M., Hersen, P., 2011. The Dynamical Systems Properties
766 of the HOG Signaling Cascade. *J. Signal Transduct.* 2011, 930940.
767 doi:10.1155/2011/930940
- 768 Mitchell, A., Wei, P., Lim, W.A., 2015. Oscillatory stress stimulation uncovers an Achilles' heel of
769 the yeast MAPK signaling network. *Science* 350, 1379–1383.
770 doi:10.1126/science.aab0892
- 771 Muzzey, D., Gómez-Uribe, C.A., Mettetal, J.T., van Oudenaarden, A., 2009. A systems-level
772 analysis of perfect adaptation in yeast osmoregulation. *Cell* 138, 160–171.
773 doi:10.1016/j.cell.2009.04.047
- 774 Nagiec, M.J., Dohlman, H.G., 2012. Checkpoints in a yeast differentiation pathway coordinate
775 signaling during hyperosmotic stress. *PLoS Genet.* 8, e1002437.
776 doi:10.1371/journal.pgen.1002437
- 777 O'Rourke, S.M., Herskowitz, I., 2004. Unique and Redundant Roles for HOG MAPK Pathway
778 Components as Revealed by Whole-Genome Expression Analysis. *Mol. Biol. Cell* 15,
779 532–542.
- 780 O'Rourke, S.M., Herskowitz, I., O'Shea, E.K., 2002. Yeast go the whole HOG for the
781 hyperosmotic response. *Trends Genet.* 18, 405–412. doi:10.1016/s0168-
782 9525(02)02723-3
- 783 Petelenz-Kurdziel, E., Kuehn, C., Nordlander, B., Klein, D., Hong, K.-K., Jacobson, T., Dahl, P.,
784 Schaber, J., Nielsen, J., Hohmann, S., Klipp, E., 2013. Quantitative analysis of glycerol
785 accumulation, glycolysis and growth under hyper osmotic stress. *PLoS Comput. Biol.* 9,
786 e1003084. doi:10.1371/journal.pcbi.1003084
- 787 Purvis, J.E., Lahav, G., 2013. Encoding and decoding cellular information through signaling
788 dynamics. *Cell* 152, 945–956. doi:10.1016/j.cell.2013.02.005
- 789 Saito, H., Posas, F., 2012. Response to hyperosmotic stress. *Genetics* 192, 289–318.
790 doi:10.1534/genetics.112.140863
- 791 Schaber, J., Baltanas, R., Bush, A., Klipp, E., Colman-Lerner, A., 2012. Modelling reveals novel
792 roles of two parallel signalling pathways and homeostatic feedbacks in yeast. *Mol. Syst.*
793 *Biol.* 8, 622. doi:10.1038/msb.2012.53

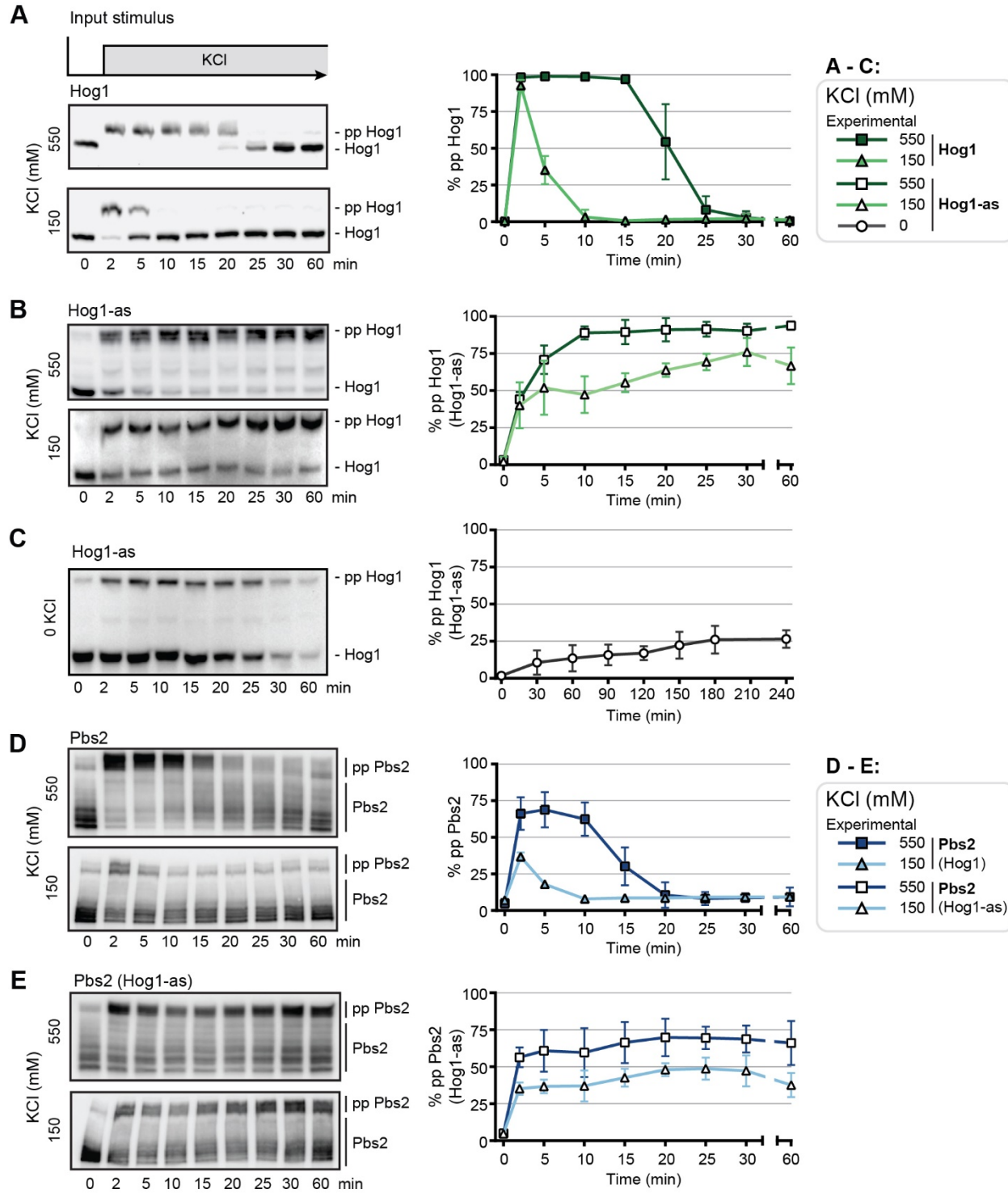
- 794 Sharifian, H., Lampert, F., Stojanovski, K., Regot, S., Vaga, S., Buser, R., Lee, S.S., Koepli, H.,
795 Posas, F., Pelet, S., Peter, M., 2015. Parallel feedback loops control the basal activity of
796 the HOG MAPK signaling cascade. *Integr Biol (Camb)* 7, 412–422.
797 doi:10.1039/c4ib00299g
- 798 Shellhammer, J.P., Morin-Kensicki, E., Matson, J.P., Yin, G., Isom, D.G., Campbell, S.L.,
799 Mohney, R.P., Dohlman, H.G., 2017. Amino acid metabolites that regulate G protein
800 signaling during osmotic stress. *PLoS Genet.* 13, e1006829.
801 doi:10.1371/journal.pgen.1006829
- 802 Siderius, M., Van Wuytswinkel, O., Reijenga, K.A., Kelders, M., Mager, W.H., 2000. The control
803 of intracellular glycerol in *Saccharomyces cerevisiae* influences osmotic stress response
804 and resistance to increased temperature. *Mol. Microbiol.* 36, 1381–1390.
805 doi:10.1046/j.1365-2958.2000.01955.x
- 806 Stojanovski, K., Ferrar, T., Benisty, H., Uschner, F., Delgado, J., Jimenez, J., Solé, C., de
807 Nadal, E., Klipp, E., Posas, F., Serrano, L., Kiel, C., 2017. Interaction dynamics
808 determine signaling and output pathway responses. *Cell Rep.* 19, 136–149.
809 doi:10.1016/j.celrep.2017.03.029
- 810 Stuckey, S., Mukherjee, K., Storici, F., 2011. In vivo site-specific mutagenesis and gene collage
811 using the delitto perfetto system in yeast *Saccharomyces cerevisiae*. *Methods Mol. Biol.*
812 745, 173–191. doi:10.1007/978-1-61779-129-1_11
- 813 Tatebayashi, K., Yamamoto, K., Tomida, T., Nishimura, A., Takayama, T., Oyama, M., Kozuka-
814 Hata, H., Adachi-Akahane, S., Tokunaga, Y., Saito, H., 2020. Osmostress enhances
815 activating phosphorylation of Hog1 MAP kinase by mono-phosphorylated Pbs2 MAP2K.
816 *EMBO J.* e103444. doi:10.15252/embj.2019103444
- 817 Thiemicke, A., Jashnsaz, H., Li, G., Neuert, G., 2019. Generating kinetic environments to study
818 dynamic cellular processes in single cells. *Sci. Rep.* 9, 10129. doi:10.1038/s41598-019-
819 46438-8
- 820 Toni, T., Welch, D., Strelkowa, N., Ipsen, A., Stumpf, M.P.H., 2009. Approximate Bayesian
821 computation scheme for parameter inference and model selection in dynamical systems.
822 *J. R. Soc. Interface* 6, 187–202. doi:10.1098/rsif.2008.0172
- 823 Ubersax, J.A., Ferrell, J.E., 2007. Mechanisms of specificity in protein phosphorylation. *Nat.*
824 *Rev. Mol. Cell Biol.* 8, 530–541. doi:10.1038/nrm2203
- 825 Villaverde, A.F., Fröhlich, F., Weindl, D., Hasenauer, J., Banga, J.R., 2019. Benchmarking
826 optimization methods for parameter estimation in large kinetic models. *Bioinformatics* 35,
827 830–838. doi:10.1093/bioinformatics/bty736
- 828 Warmka, J., Hanneman, J., Lee, J., Amin, D., Ota, I., 2001. Ptc1, a type 2C Ser/Thr
829 phosphatase, inactivates the HOG pathway by dephosphorylating the mitogen-activated
830 protein kinase Hog1. *Mol. Cell. Biol.* 21, 51–60. doi:10.1128/MCB.21.1.51-60.2001
- 831 Westfall, P.J., Thorner, J., 2006. Analysis of mitogen-activated protein kinase signaling
832 specificity in response to hyperosmotic stress: use of an analog-sensitive HOG1 allele.
833 *Eukaryotic Cell* 5, 1215–1228. doi:10.1128/EC.00037-06

- 834 Wurgler-Murphy, S.M., Maeda, T., Witten, E.A., Saito, H., 1997. Regulation of the
835 *Saccharomyces cerevisiae* HOG1 mitogen-activated protein kinase by the PTP2 and
836 PTP3 protein tyrosine phosphatases. Mol. Cell. Biol. 17, 1289–1297.
837 doi:10.1128/mcb.17.3.1289
- 838 Yamamoto, K., Tatebayashi, K., Tanaka, K., Saito, H., 2010. Dynamic control of yeast MAP
839 kinase network by induced association and dissociation between the Ste50 scaffold and
840 the Opy2 membrane anchor. Mol. Cell 40, 87–98. doi:10.1016/j.molcel.2010.09.011
- 841 Zi, Z., Liebermeister, W., Klipp, E., 2010. A quantitative study of the Hog1 MAPK response to
842 fluctuating osmotic stress in *Saccharomyces cerevisiae*. PLoS One 5, e9522.
843 doi:10.1371/journal.pone.0009522
- 844
- 845
- 846
- 847
- 848
- 849
- 850
- 851
- 852
- 853
- 854
- 855
- 856



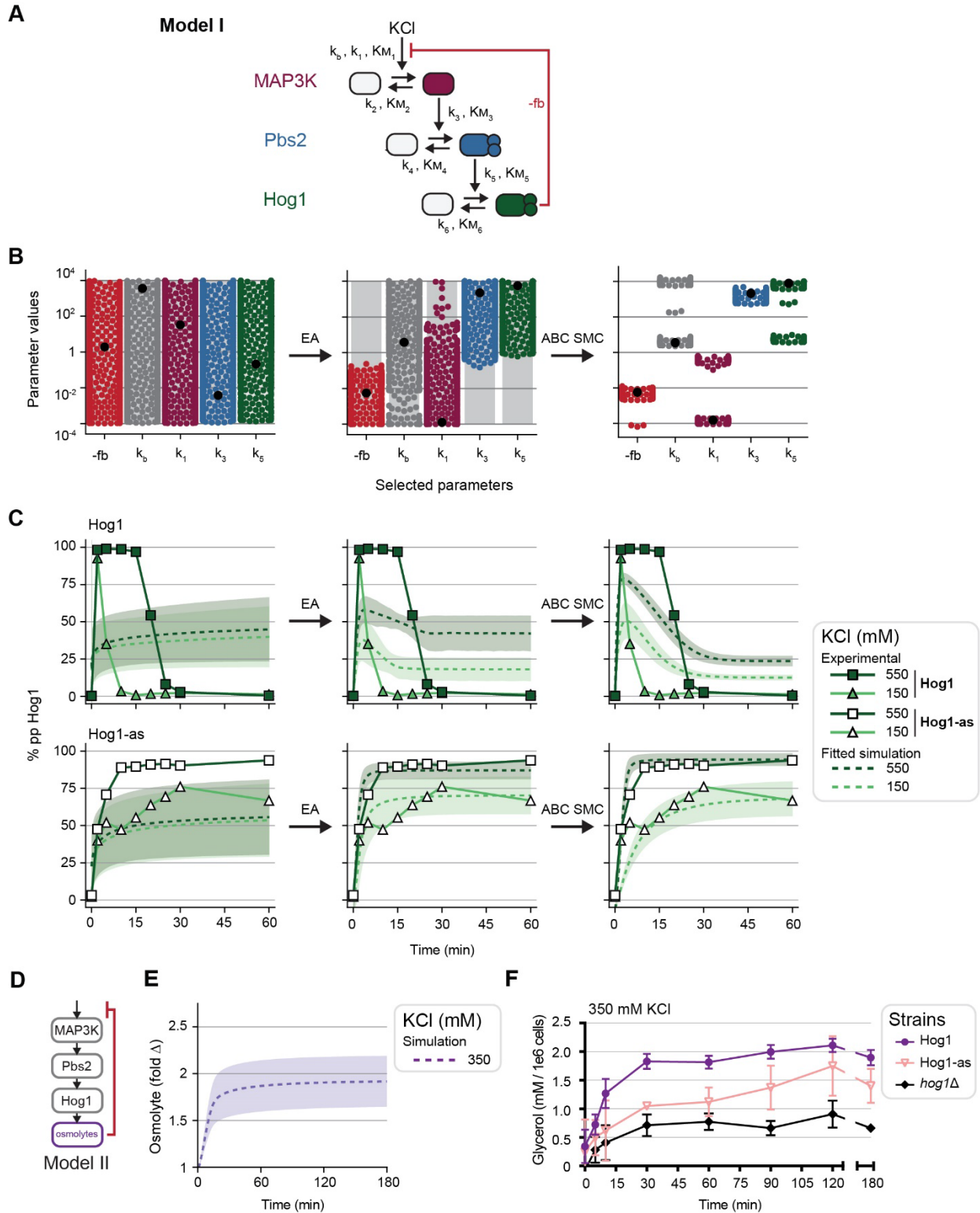
857

858 **Figure 1: Hog1-dependent feedbacks within the HOG Pathway.** Two input branches activate a MAPK cascade to
859 initiate adaptation to hyperosmotic stress. Hog1 controls its own phosphorylation dynamics through negative (red
860 arrows) and positive (green arrow) feedback mechanisms. Hog1 phosphorylates upstream HOG pathway
861 components, including Ste11, Ssk2, and Sho1, which downregulates signaling. Hog1 increases osmolyte
862 concentrations by cytosolic and nuclear events, such as the closing of glycerol export channels and the transcription
863 of genes with Stress Response Elements (SREs). The increase of intracellular osmolarity also suppresses HOG
864 signaling, putatively at the level of receptors. Finally, Hog1 likely initiates a positive feedback loop, but the target is
865 still unknown.



866

867 **Figure 2: HOG pathway dynamics.** (A) Left: Hog1 dual phosphorylation (pp Hog1) over time in response to a single
868 step stimulus (top) of 550 mM KCl (center) or 150 mM KCl (bottom), resolved using the Phos-tag method. Right:
869 Quantification of blots. (B) Same as (A) but using an analog sensitive Hog1 + ATP analog (Hog1-as). (C) Same as
870 (B) but taken for longer time points and in the absence of KCl. (D) Left: Pbs2 phosphorylation over time in response
871 to 550 mM KCl (top) and 150 mM KCl (bottom), resolved using the Phos-tag method. (E) Same as (D) but using
872 Hog1-as. Error bars represent SD of each point. All experimental data are n = 3.



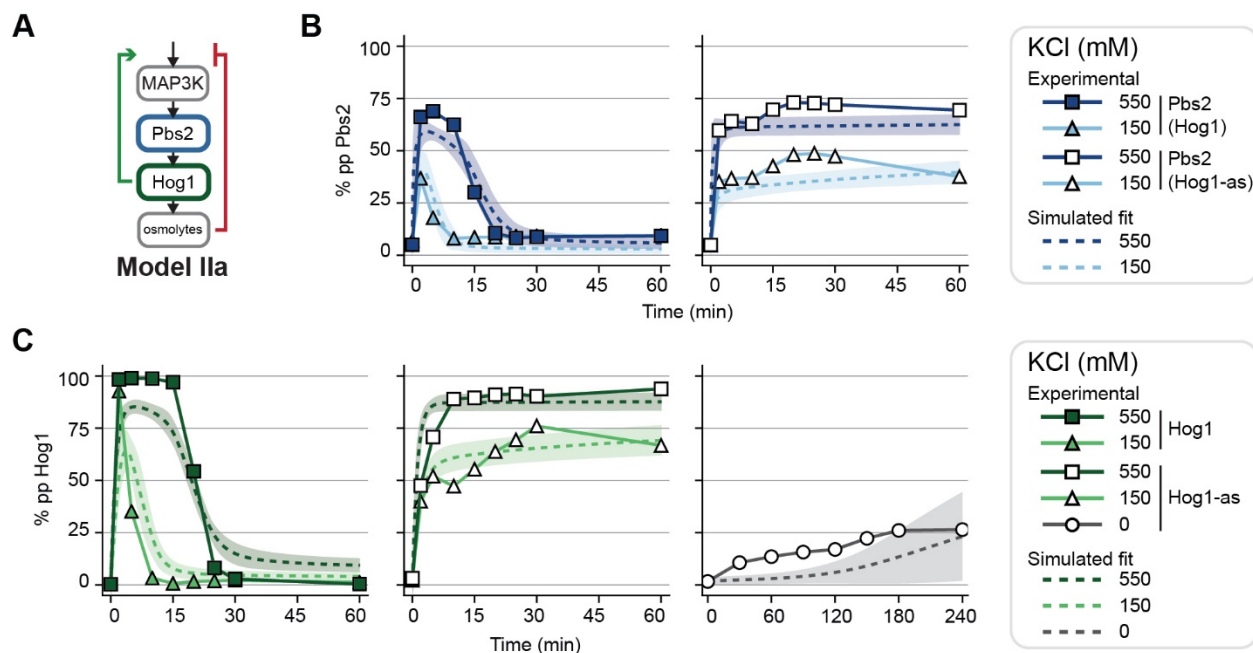
873

874 **Figure 3: Model building and parameter estimation of potential feedback circuits. (A)** Schematic of Model I, a
875 single negative feedback from Hog1, targeting the input with associated parameters to be estimated. **(B)** The
876 parameter optimization method. First, parameter values are randomly assigned, then the Evolutionary Algorithm (EA)
877 finds candidate parameter sets, and finally, the Approximate Bayesian Computation Sequential Monte Carlo (ABC

878 SMC) searches the local parameter space surrounding the EA parameter sets. Gray bars indicate the range of
879 potential values selected uniformly during the EA. Colored points specify parameter values and black points highlight
880 the best (lowest MSE between experimental data and simulations) parameter values after each step. **(C)** Simulated
881 fits at each estimation step are overlaid with wildtype Hog1 (top row, filled symbols) and Hog1-as (bottom row, open
882 symbols) data at each parameter optimization step. Average simulated behaviors are plotted using dashed lines. All
883 simulations are $n = 1000$ and all shaded regions are a SD of 1. **(D)** Schematic of Model II that features a delayed
884 negative feedback, presumably from osmolyte accumulation. **(E)** Model II simulated prediction of downstream
885 component behavior. **(F)** Glycerol accumulation over time in response to 350 mM KCl with and without Hog1 activity.
886 *hog1Δ* cells served as a negative control. All experiments are $n = 3$ and error bars represent SD of each point.

887

888



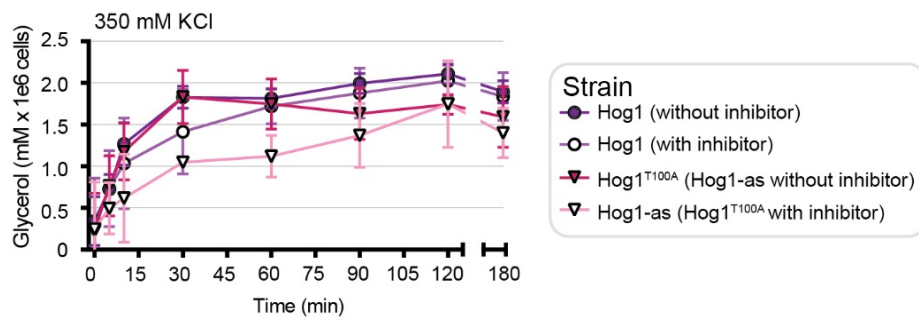
889

890 **Figure 3 – figure supplement 1: Model II (delayed negative feedback) fits to experimental data.** **(A)** Schematic
891 of Model II with negative feedback driven by a species downstream of Hog1, such as Hog1-dependent accumulation
892 of osmolytes. **(B)** Model II simulated Pbs2 fits (dashed lines) overlaid with data (symbols). Left: Data and simulations
893 for wildtype Hog1 in response to 550 mM and 150 mM KCl. Right: Data and simulations for Hog1-as. **(C)** Model II
894 simulated Hog1 fits (dashed lines) overlaid with data (symbols). Left: Data and simulations for wildtype Hog1 in
895 response to 550 mM and 150 mM KCl. Center: Data and simulations for Hog1-as. Right: Data and simulations for
896 Hog1-as with no salt stimulus. All simulations in (B) and (C) are $n = 1000$ and shaded regions are SD of 1.

897

898

899

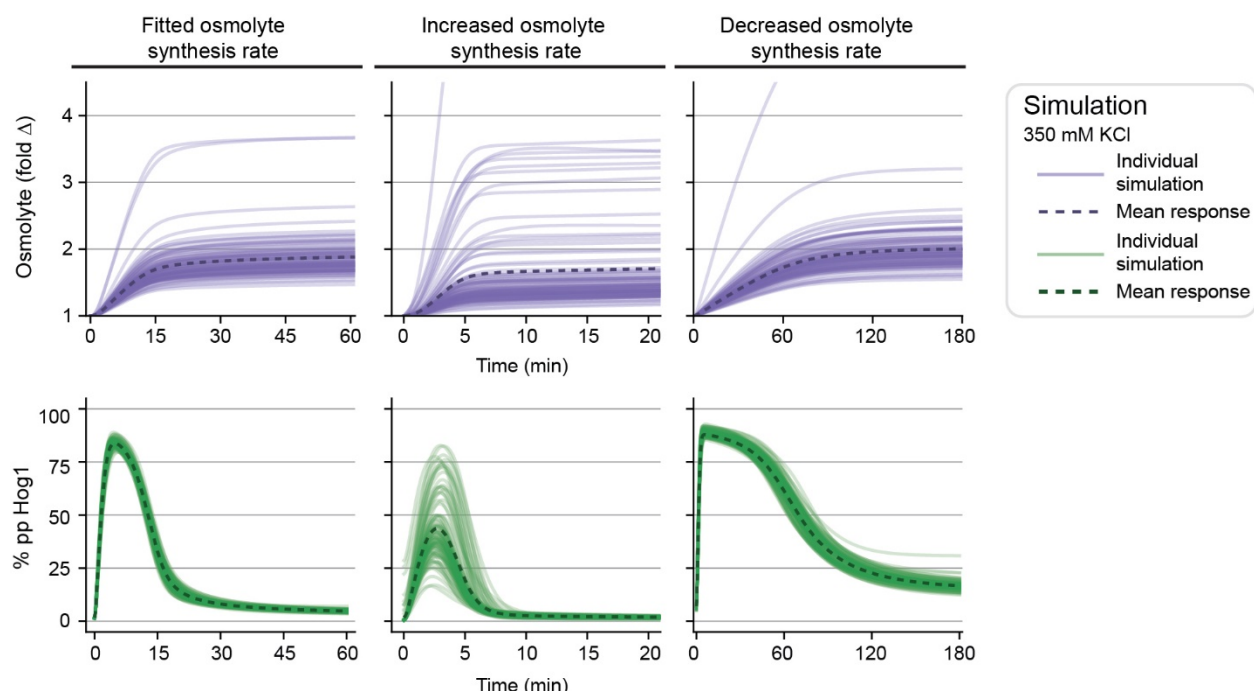


900

901 **Figure 3 – figure supplement 2: Inhibitor- and Hog1 analog sensitive variant-dependent glycerol**
902 **accumulation in response to hyperosmotic stress.** Glycerol accumulation over time in response to 350 mM KCl
903 with and without 1-NA-PP1 drug in both wildtype Hog1 and Hog1^{T100A} backgrounds. All experiments are $n = 3$ and
904 error bars represent SD of each point.

905

906



907

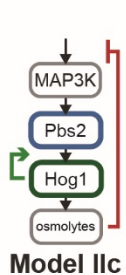
908

909 **Figure 3 – figure supplement 3: Delayed feedback investigation.** Comparing Model II simulations with the fitted
910 (left) osmolyte synthesis rate to 5x increased (center) or 5x decreased (right) osmolyte synthesis rate in response to
911 350 mM KCl. Each solid line is one simulation corresponding to one fitted parameter set and each dashed line is the
912 mean response of the plotted simulations. Top row is osmolyte simulations (purple) and bottom row is the
913 corresponding Hog1 simulations (green). The best 100 simulations are plotted for clear visualization.

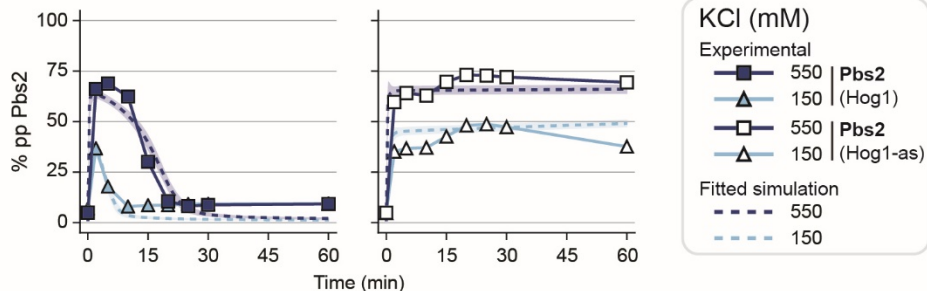
A

Data fit to:	Strain	Phosphorylation Characteristic	Model:							
			I	Ia	Ib	Ic	II	IIa	IIb	IIc
	Hog1	(1) fast / full								
		(2) transient	○	○	○	○	○	○	●	●
		(3) no basal	○	○	○	○	●	●	●	●
	Hog1-as	(4) slow / partial	●	●	●	●	●	○	●	●
		(5) sustained	●	●	●	●	●	●	●	●
		(6) basal	○	○	○	○	○	●	●	●
	Hog1	(7) fast / partial	○	○	○	○	○	●	●	●
		(8) transient	○	○	○	○	○	●	●	●
	Hog1-as	(9) fast / partial	○	○	○	○	○	●	●	●
		(10) sustained	●	●	●	●	●	●	●	●

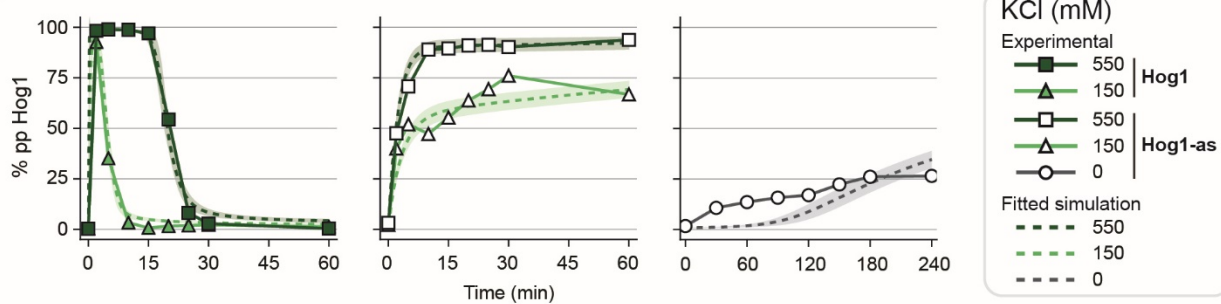
B



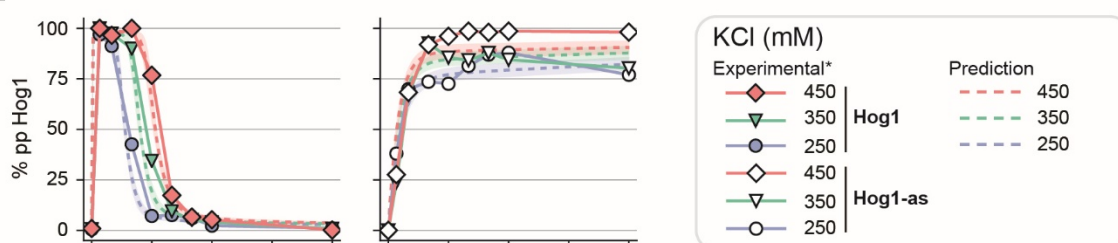
C



D



E



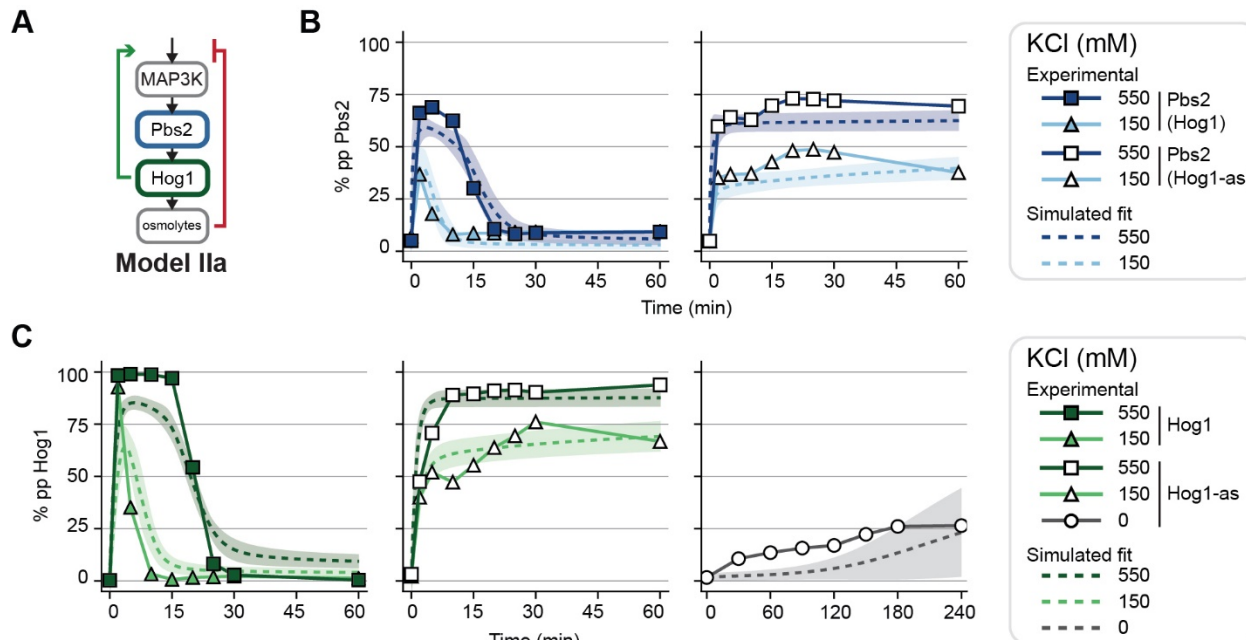
914

915 **Figure 4: Model fits and predictions to single step stimuli. (A)** Table showing model fits to each of the HOG
916 pathway characteristics. Dots indicate that the model captures the behavior, where filled circles fit the experimental
917 data well and hollow circles do not. **(B)** Schematic of one of the two models that fits all of the phosphorylation
918 characteristics. **(C)** Model IIc simulated Pbs2 fits (dashed lines) overlaid with experimental data (symbols). Left: Data
919 and simulations for wildtype Hog1 in response to 550 mM and 150 mM KCl. Right: Data and simulations for Hog1-as.
920 **(D)** Model IIc simulated Hog1 fits (dashed lines) overlaid with experimental data (symbols). Left: Data and simulations
921 for wildtype Hog1 in response to 550 mM and 150 mM KCl. Center: Data and simulations for Hog1-as. Right: Data

922 and simulations for Hog1-as with no salt stimulus. All simulations are $n = 1000$ and shaded regions are SD = 1. **(E)**
923 Model IIc predictions to previously published data (*English et al., 2015). Left: Data and simulations for wildtype Hog1
924 in response to 450, 350, 250 mM KCl. Right: Data and simulations for wildtype Hog1-as.

925

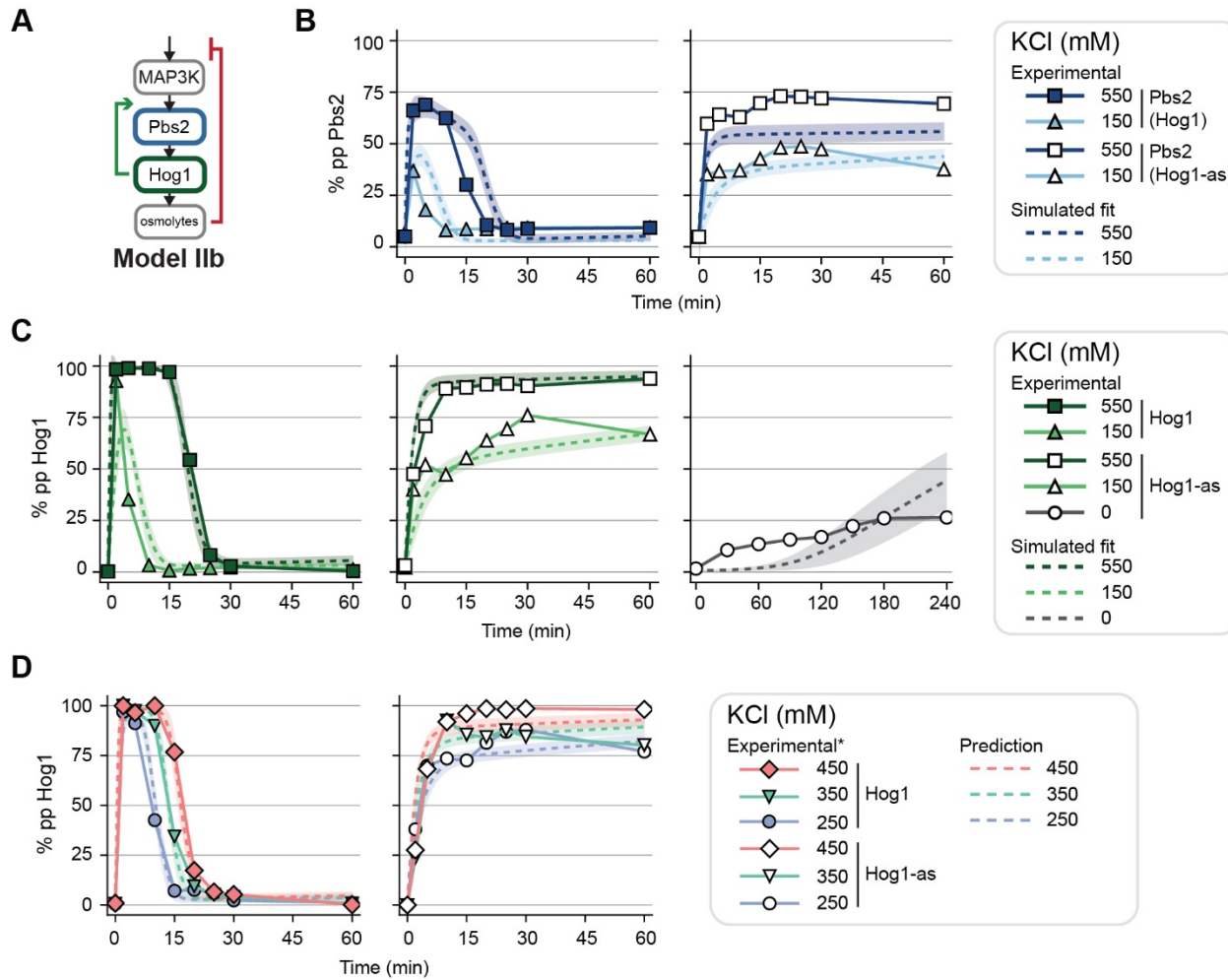
926



927

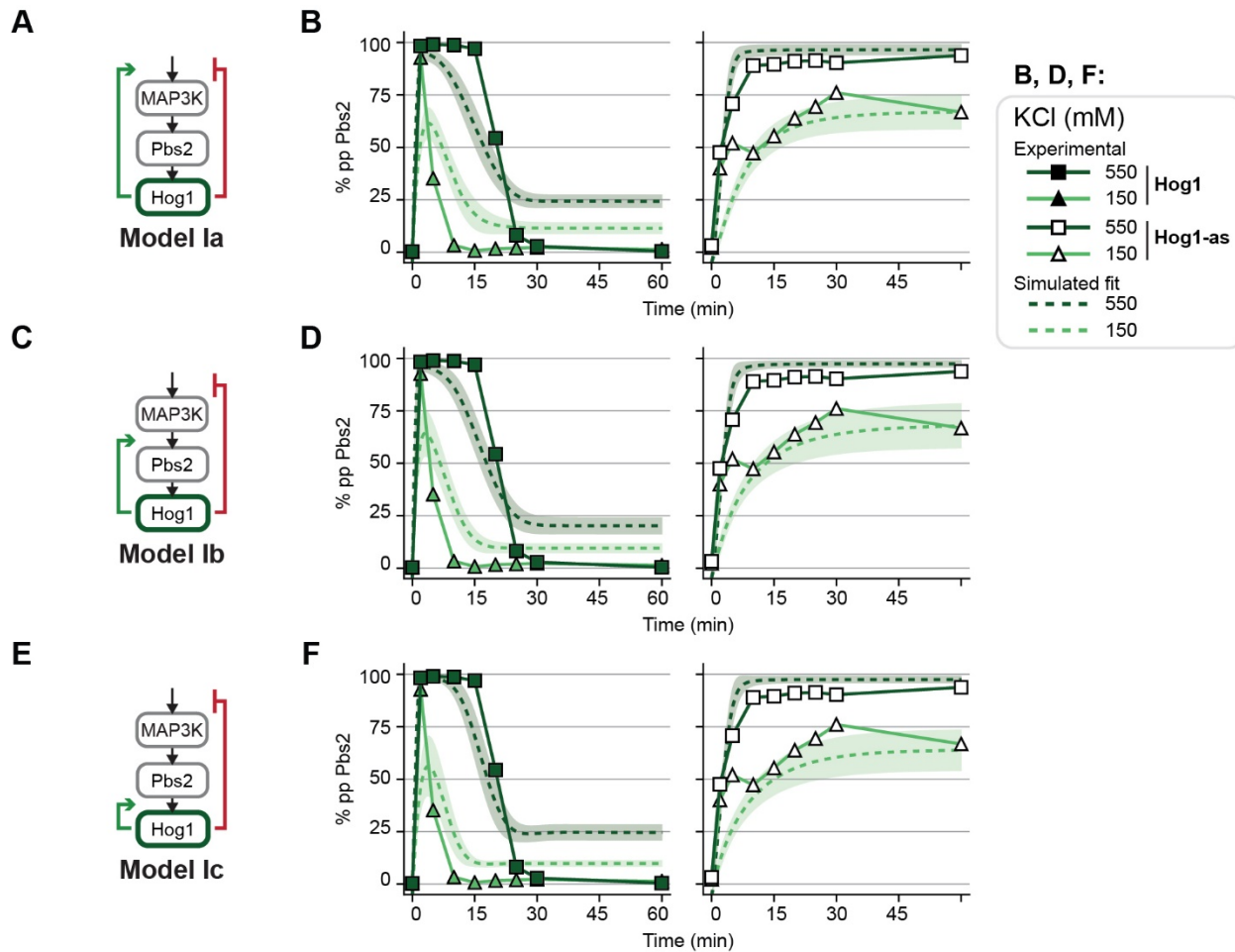
928 **Figure 4 – figure supplement 1: Model IIa with positive and negative feedback poorly fits experimental data.**
929 **(A)** Schematic of Model IIa with a delayed negative feedback and a positive feedback increasing MAP3K activation.
930 **(B)** Model IIa simulated Pbs2 fits (dashed lines) overlaid with data (symbols). Left: Data and simulations for wildtype
931 Hog1 in response to 550 mM and 150 mM KCl. Right: Data and simulations for Hog1-as. **(C)** Model IIa simulated
932 Hog1 fits (dashed lines) overlaid with data (symbols). Left: Data and simulations for wildtype Hog1 in response to 550
933 mM and 150 mM KCl. Center: Data and simulations for Hog1-as. Right: Data and simulations for Hog1-as with no salt
934 stimulus.

935



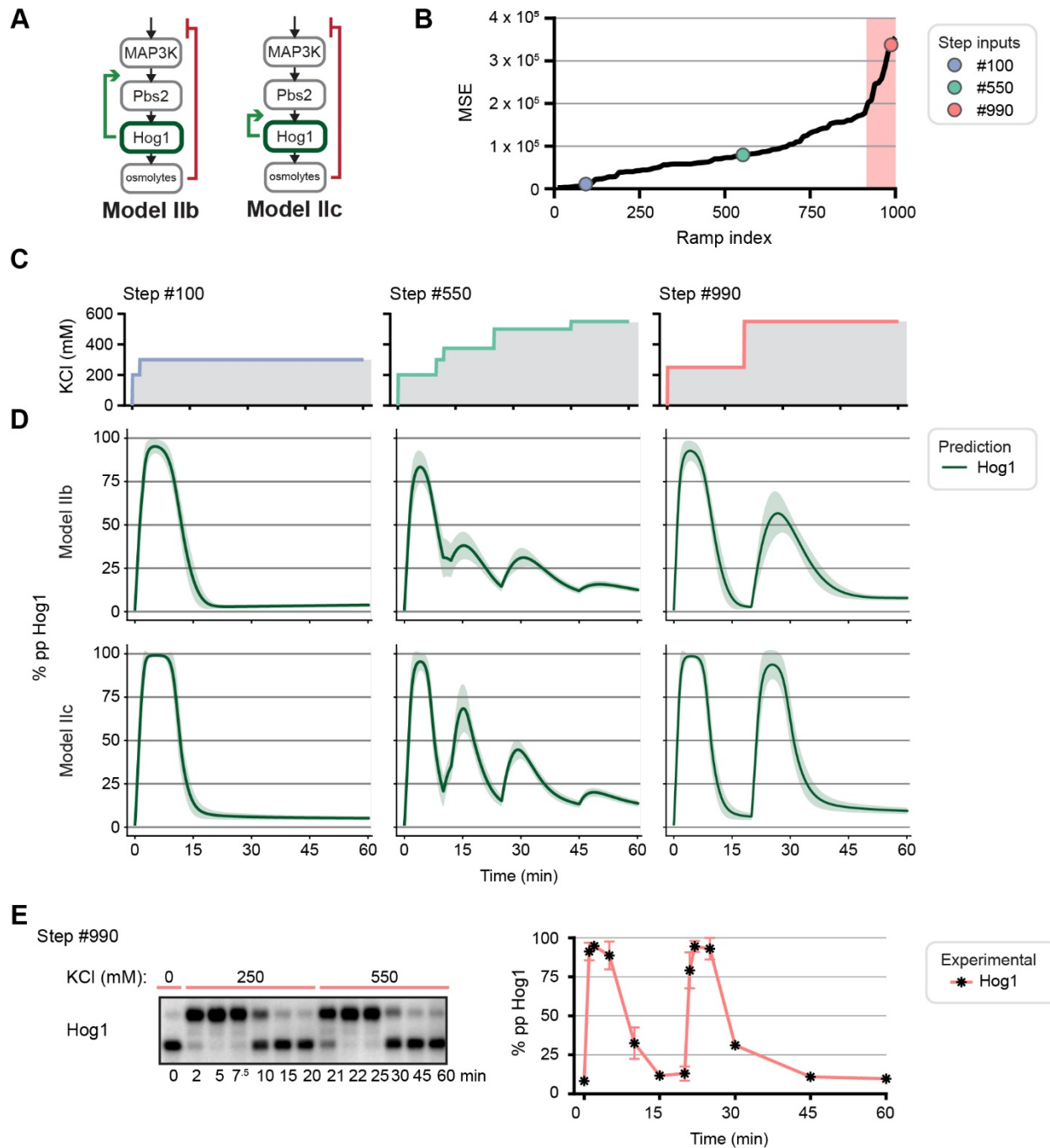
936
937
938
939
940
941
942
943
944
945

Figure 4 – figure supplement 2: Model IIb with positive and negative feedback that captures experimental data. (A) Schematic of Model IIb with a delayed negative feedback and a positive feedback increasing MAP2K activation. (B) Model IIa simulated Pbs2 fits (dashed lines) overlaid with data (symbols). Left: Data and simulations for wildtype Hog1 in response to 550 mM and 150 mM KCl. Right: Data and simulations for Hog1-as. (C) Model IIa simulated Hog1 fits (dashed lines) overlaid with data (symbols). Left: Data and simulations for wildtype Hog1 in response to 550 mM and 150 mM KCl. Center: Data and simulations for Hog1-as. Right: Data and simulations for Hog1-as with no salt stimulus. (D) Model IIb predictions to *previously published data (English et al., 2015). Left: Data and simulations for wildtype Hog1 in response to 450, 350, 250 mM KCl. Right: Data and simulations for wildtype Hog1-as. All simulations are $n = 1000$ and shaded regions represent a SD of 1.



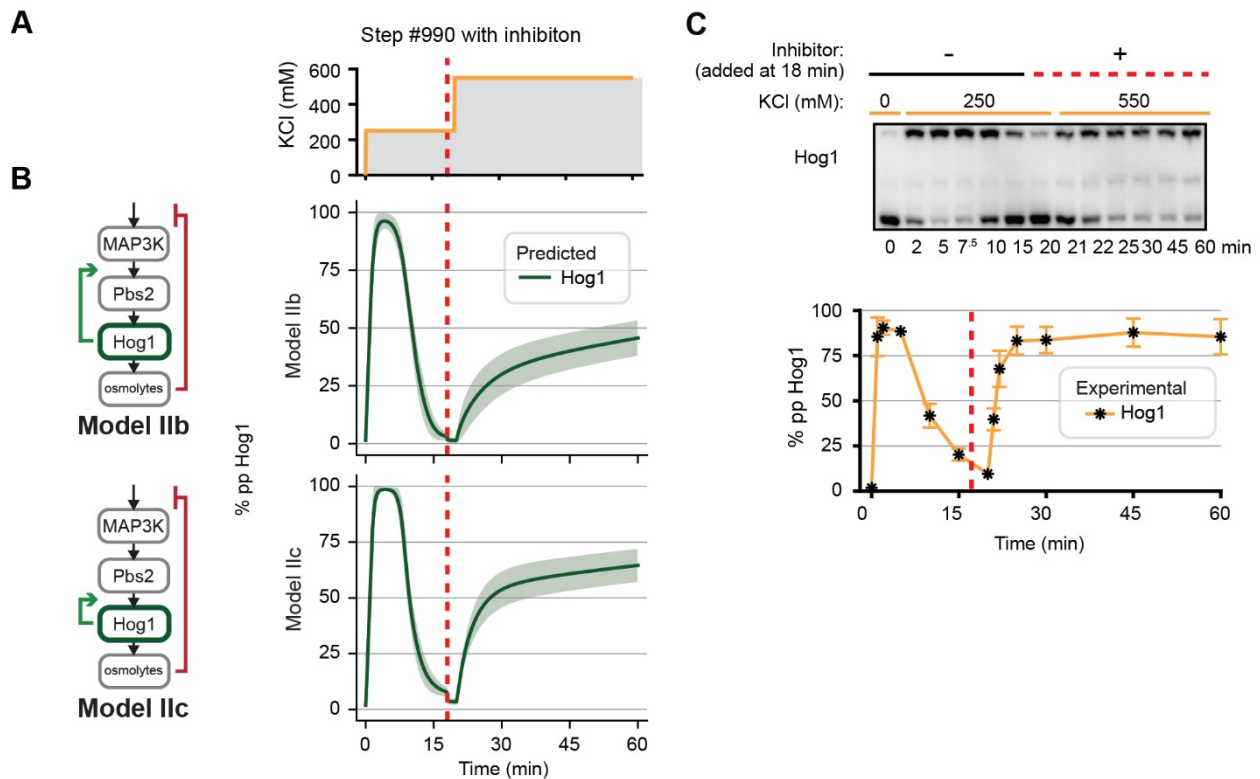
946

947 **Figure 4 – figure supplement 3: Models with direct negative feedback and positive feedback cannot capture**
 948 **experimental data. (A)** Schematic of Model Ia with a negative feedback directly from Hog1 and a positive feedback
 949 increasing MAP3K activation. **(B)** Model Ia simulated Hog1 fits overlaid with data. Data and simulations for wildtype
 950 Hog1 in response to 550 mM and 150 mM KCl. Right: Data and simulations for Hog1-as. **(C)** Schematic of Model Ib
 951 with a negative feedback directly from Hog1 and a positive feedback increasing MAP2K activation. **(D)** Same as (B)
 952 but for Model Ib. **(E)** Schematic of Model Ic with a negative feedback directly from Hog1 and a positive feedback
 953 increasing MAPK activation. **(F)** Same as (B) but for Model Ic. All simulations are n = 1000 and shaded regions
 954 represent a SD of 1.



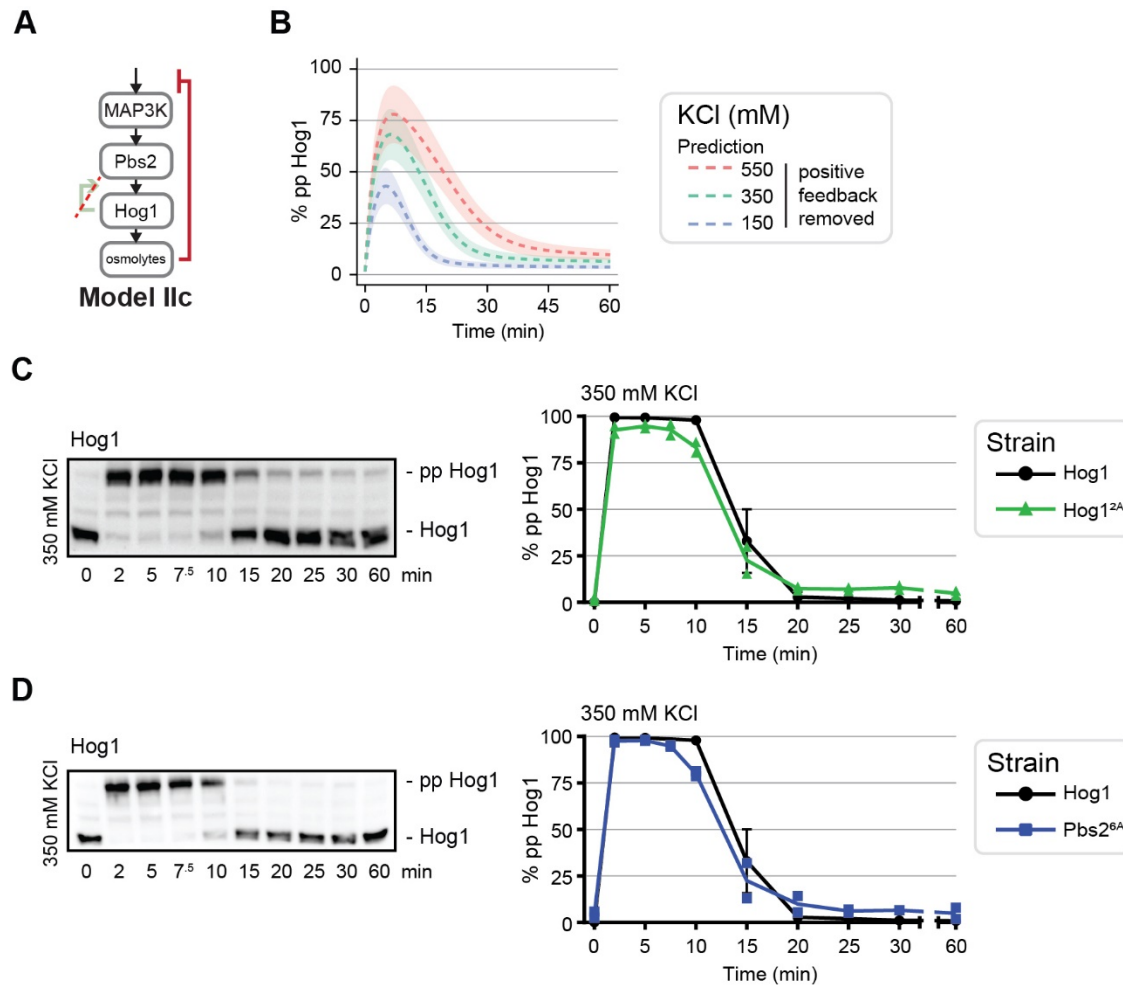
955
956
957
958
959
960
961
962

Figure 5: Differentiating models by predicting Hog1 behaviors to dynamic inputs. (A) Schematics of the two models that fit our data. (B) Mean squared errors (MSEs) for the predicted Hog1 behaviors of Models IIb and IIc for 1000 randomly generated increasing steps. Pink shaded area indicates where step inputs follow a trend similar to that of Steps #990 (pink circle). (C) Selected steps depicting a low (left), mid (center), and high (right) scoring step input. (D) Predicted Hog1 behaviors to the three step inputs for Models IIb (mid), and IIc (bottom) (C). (E) Experimental Hog1 behavior to step stimulus. Left: Hog1 behavior in response to Step #990 resolved using Phos-tag SDS-PAGE (n=3). Right: Quantification of blots. Error bar represent SD of each point.



963

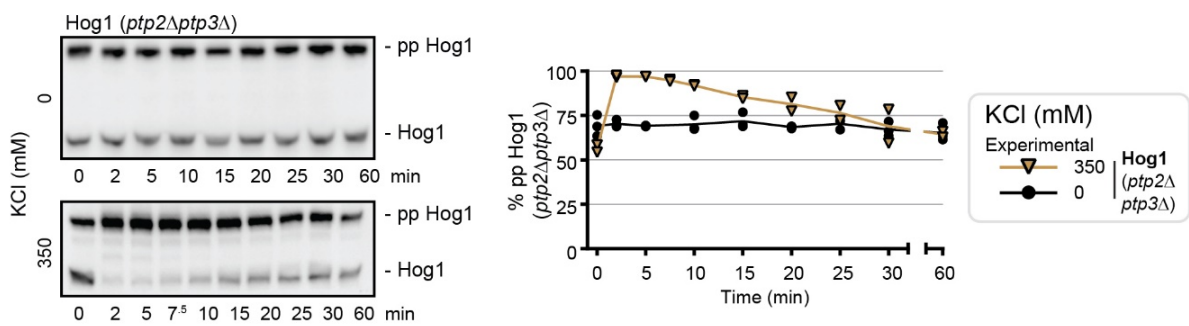
964 **Figure 5 – figure supplement 1: Model and experimental Hog1 behavior in response to step stimulus and**
 965 **inhibition.** (A) Step stimulus #990 with inhibition before the second step of inhibition ($t=18$ min). (B) Model
 966 predictions to step stimulus with the inhibition. Top: Model IIb prediction. Bottom: Model IIC prediction. (C)
 967 Experimental Hog1 behavior to the stimulus. Top: Hog1 behavior in response to Step #990 resolved using Phos-tag
 968 SDS-PAGE ($n=3$). Bottom: Quantification of blots. Error bar represent SD of each point.



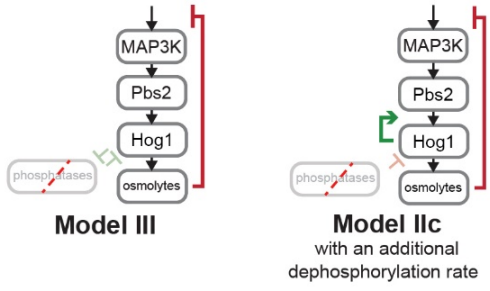
969

970 **Figure 6: Evaluating increasing Hog1 phosphorylation as the positive feedback mechanism.** (A) Schematic of
971 Model IIc with positive feedback removed. (B) Model IIc prediction of Hog1 in response to 550, 350, and 150 mM KCl
972 without positive feedback. (C) Left: Hog1 behavior in response to 350 mM KCl with putative MAPK consensus sites
973 mutated in Pbs2. Right: Quantification of blots. (D) Left: Hog1 behavior in response to 350 mM KCl with putative
974 MAPK consensus sites mutated in Hog1. Right: Quantification of blots. n = 2 for mutants, points are replicates and
975 line is mean; n = 3 for wildtype Hog1, points and line are mean with SD.

A

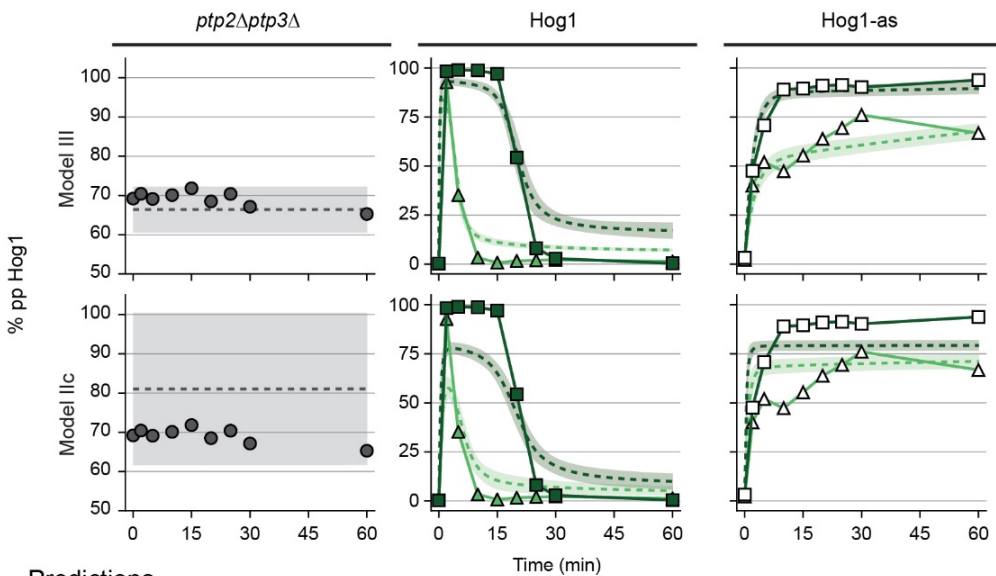


B



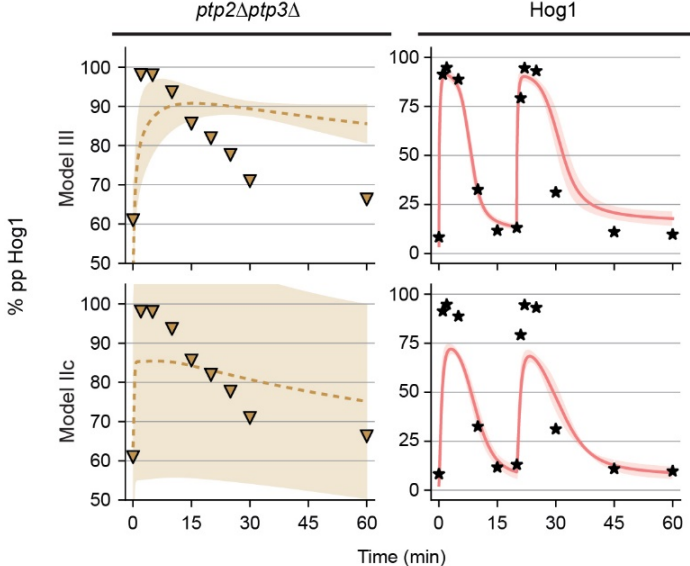
C

Fitted simulations



D

Predictions



C - D:

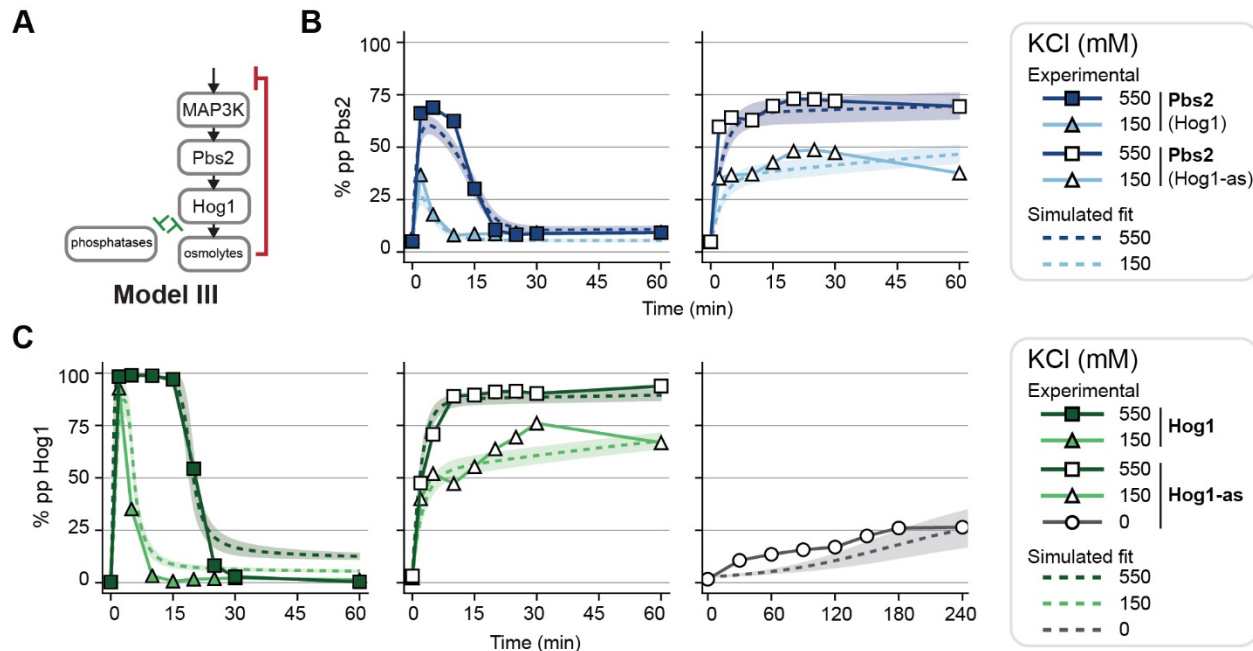
KCl (mM)	Experiment	Simulation	Hog1 ($\text{ptp2}^{\Delta}\text{ptp3}^{\Delta}$)
0	●	-	-
350	▼	-	-
550	-	— (green)	-
150	-	-	-
Steps #990	-	-	-
550	-	-	-
150	-	-	-

KCl (mM)	Experiment	Simulation	Hog1
0	●	-	-
350	▼	-	-
550	-	— (green)	-
150	-	-	-

KCl (mM)	Experiment	Simulation	Hog1-as
0	●	-	-
350	▼	-	-
550	-	— (green)	-
150	-	-	-

977 **Figure 7: Evaluating decreasing Hog1 dephosphorylation as the positive feedback mechanism. (A)** Left: Hog1
978 behavior in response to 350 mM KCl and no KCl in a *ptp2Δptp3Δ* background. Right: Quantification of blots. n=2,
979 points are replicates and line is mean. **(B)** Schematic of models incorporating phosphatases. Left: Model III, with
980 positive feedback acts through mutual inhibition between Hog1 and its phosphatases. Right: Model IIc, with an
981 additional dephosphorylation rate to simulate the removal of the phosphatases. **(C)** Model fits to experimental data
982 (selective representatives shown). Top: Model III. Left: Simulated Hog1 fits to *ptp2Δptp3Δ* without KCl stimulus.
983 Center: Fits to wildtype Hog1 dynamics for 550 and 150 mM KCl. Right: Fits to Hog1-as data. Bottom: Same as Top
984 but for Model IIc. **(D)** Model predictions compared to experimental data. Top: Model III. Left: Prediction of Hog1
985 dynamics in response to 350 mM KCl in a *ptp2Δptp3Δ* background. Right: Prediction in response to Steps #990.
986 Bottom: Same as Top but for Model IIc.

987



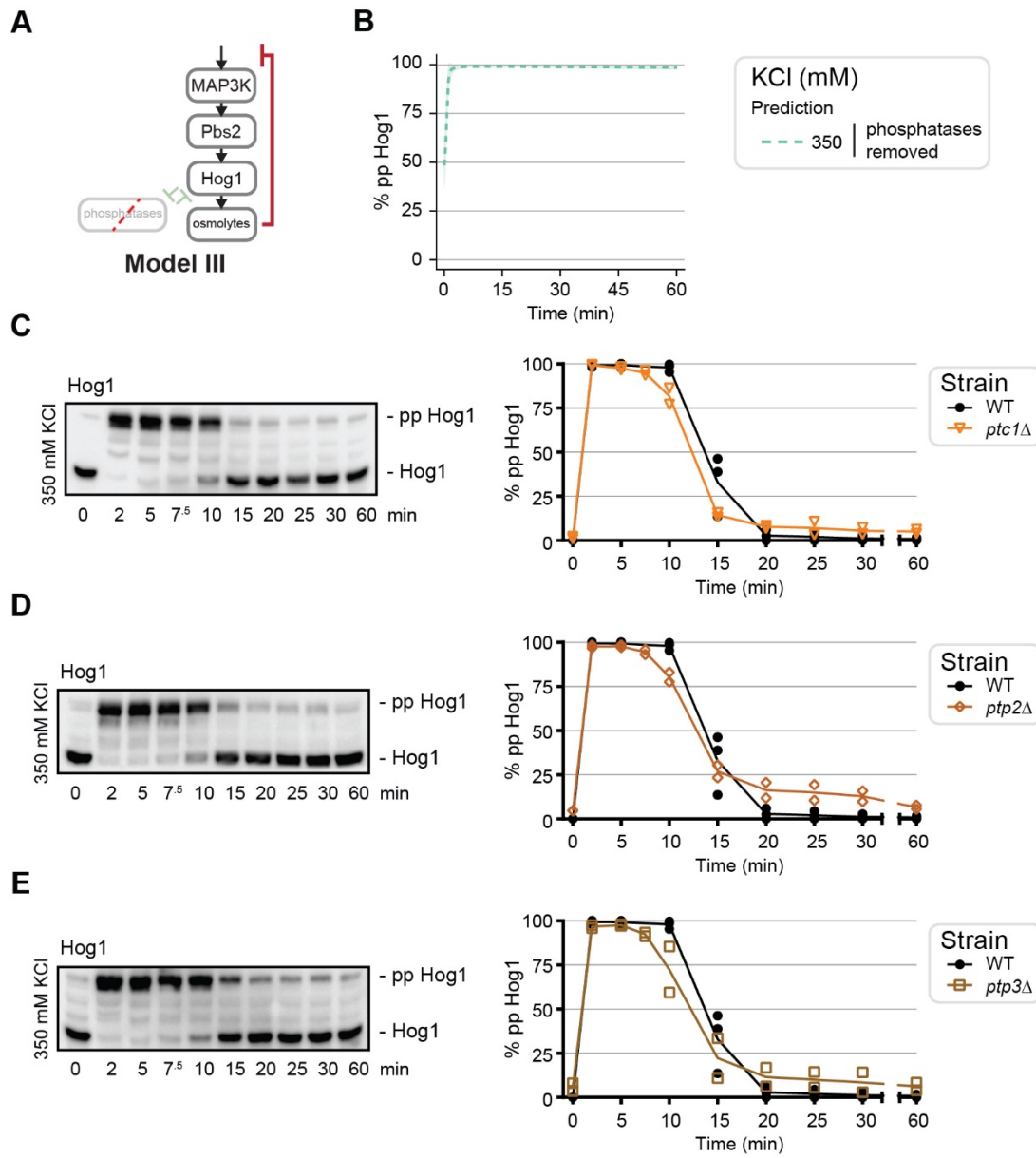
989 **Figure 7 – figure supplement 1: Model III with positive feedback acting through mutual inhibition captures**
990 **experimental data. (A)** Schematic of Model III with a delayed negative feedback and a positive feedback decreasing
991 its phosphatases' activity. **(B)** Model III simulated Pbs2 fits (dashed lines) overlaid with data (symbols). Left: Data and
992 simulations for wildtype Hog1 in response to 550 mM and 150 mM KCl. Right: Data and simulations for Hog1-as. **(C)**
993 Model IIa simulated Hog1 fits (dashed lines) overlaid with data (symbols). Left: Data and simulations for wildtype
994 Hog1 in response to 550 mM and 150 mM KCl. Center: Data and simulations for Hog1-as. Right: Data and
995 simulations for Hog1-as with no salt stimulus. All simulations are n = 1000 and shaded regions represent a SD of 1.

996

997

998

999



1000

1001 **Figure 7 – figure supplement 2: Single deletions of the primary Hog1 phosphatases slightly decrease**
1002 **duration of Hog1 activation. (A)** Schematic of Model III with mutual inhibition acting as positive feedback, here
1003 depicted as the phosphatases removed. **(B)** Model III Hog1 prediction in response to 350 mM KCl if the
1004 phosphatases were removed. Simulations are n = 1000 and shaded regions represent a SD of 1. **(C)** Left: Hog1
1005 behavior in response to 350 mM KCl in ptc1Δ background. Right: Quantification of blots. **(D)** Same as (A) for ptp2Δ
1006 background. **(E)** Same as (A) for ptp3Δ background.